AD-A194 144 WAVE PROPAGATION AND VIBRATION OF FIBRE REINFORCED LAMINATES(U) NOTTINGHAM UNIV (ENGLAND) DEPT OF THEORETICAL MECHANICS W A GREEN ET AL. 31 AUG 87 1/1

UNCLASSIFIED AFOSR-86-0330 F/G 11/4 NL

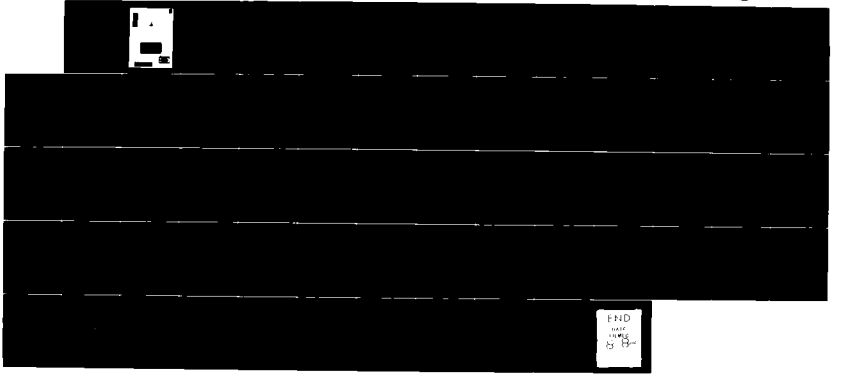

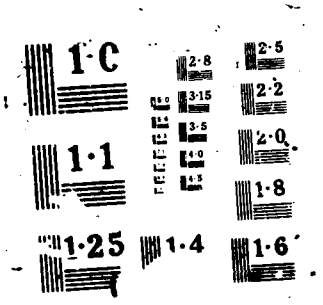
1·C
1·1
1·25
2·8
3·15
3·5
4·0
4·5
1·4
2·5
2·2
2·0
1·8
1·6

(2)

UNIVERSITY OF NOTTINGHAM

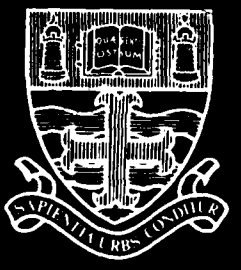

DEPARTMENT OF THEORETICAL MECHANICS

FINAL SCIENTIFIC REPORT ON GRANT NUMBER

AFOSR - 86 - 0330

(2)

FINAL SCIENTIFIC REPORT ON GRANT NUMBER

AFOSR - 86 - 0330

C&H

UNCLASSIFIED
SECURITY CLASSIFICATION OF THIS PAGE

A194144

REPORT DOCUMENTATION PAGE

1a REPORT SECURITY CLASSIFICATION UNCLASSIFIED	1b RESTRICTIVE MARKINGS
2a SECURITY CLASSIFICATION AUTHORITY	3 DISTRIBUTION / AVAILABILITY OF REPORT Approved for public release; Distribution unlimited
2b DECLASSIFICATION / DOWNGRADING SCHEDULE	
4 PERFORMING ORGANIZATION REPORT NUMBER(S)	5 MONITORING ORGANIZATION REPORT NUMBER(S)
6a NAME OF PERFORMING ORGANIZATION Nottingham University 6b OFFICE SYMBOL (If applicable)	7a NAME OF MONITORING ORGANIZATION European Office of Aerospace Research and Development (EOARD)
6c ADDRESS (City, State, and ZIP Code) University Park, Nottingham, NG7 2RD United Kingdom	7b ADDRESS (City, State, and ZIP Code) 223/231 Old Marylebone Road London NW1 5TH United Kingdom
8a NAME OF FUNDING / SPONSORING ORGANIZATION European Office of Aerospace Research & Developmt 8b OFFICE SYMBOL (If applicable) LDS	9 PROCUREMENT INSTRUMENT IDENTIFICATION NUMBER AFOSR-86-0330
8c ADDRESS (City, State, and ZIP Code) Box 14 FPO NY 09510	10 SOURCE OF FUNDING NUMBERS PROGRAM ELEMENT NO: 61102F; PROJECT NO: 2301; TASK NO: D1; WORK UNIT ACCESSION NO: 215
11 TITLE (Include Security Classification) Wave Propogation and Vibration of Fibre Reinforced Laminates	
12 PERSONAL AUTHOR(S) W. A. Green and E. Rhian Bayliss	
13a TYPE OF REPORT Final	13b TIME COVERED FROM 31/8/86 TO 31/8/87
14 DATE OF REPORT (Year, Month, Day) 87/8/31	15 PAGE COUNT
16 SUPPLEMENTARY NOTATION	

17 COSATI CODES		
FIELD	GROUP	SUB-GROUP

18 SUBJECT TERMS (Continue on reverse if necessary and identify by block number)
Stress wave propagation, Impact, Fibre composites, Laminates, Transverse isotropy

19 ABSTRACT (Continue on reverse if necessary and identify by block number)

This paper deals with wave propagation in a symmetric cross-ply laminated plate due to an impulsive normal line load acting on the upper surface of the plate. The fibre-reinforced composite forming each of the four layers is modelled as a transversely isotropic homogeneous elastic continuum which is inextensible in the fibre direction. Transform methods are employed to obtain solutions of the equations of motion in each layer in terms of propagator matrices. These general solutions are combined through the interface conditions to yield expressions for the displacement and stress transforms corresponding to the impact problem. Inversion of these transforms involves numerical integration along each branch of the plate dispersion equation and summation over a total of 18 branches. Graphical results are presented which show the variation of displacement and stresses at the upper and lower surfaces of the plate as functions of position at various times after impact.

20 DISTRIBUTION / AVAILABILITY OF ABSTRACT ☐ UNCLASSIFIED/UNLIMITED ☒ SAME AS RPT ☒ DTIC USERS	21 ABSTRACT SECURITY CLASSIFICATION Unclassified
22a NAME OF RESPONSIBLE INDIVIDUAL Lt. Col James G.R. Hansen	22b TELEPHONE (Include Area Code) 44-01-409-4299 22c OFFICE SYMBOL EOARD/LDS

DD FORM 1473, 84 MAR 83 APR edition may be used until exhausted
All other editions are obsolete

SECURITY CLASSIFICATION OF THIS PAGE
UNCLASSIFIED

FINAL SCIENTIFIC REPORT ON GRANT NUMBER

AFOSR-86-0330

Principal Investigator: Dr. W. A. Green
Department of Theoretical Mechanics,
The University,
Nottingham, NG7 2RD, U.K.

Full Time Investigator: Dr. E. Rhian Baylis

Program Manager: Lt. Col. J. G. R. Hansen
EOARD
223/231 Old Marylebone Road,
London NW1 5TH, U.K.

Research Title: Wave propagation and vibration of fibre reinforced laminates

Start date: August 31st 1986

End date: August 30th 1987

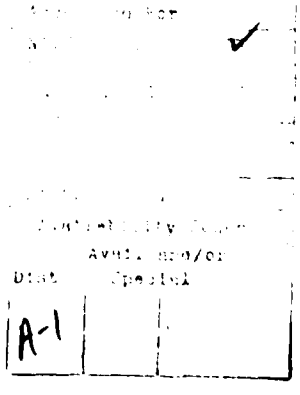

IMPACT STRESS WAVES IN FIBRE-REINFORCED LAMINATED PLATES

by

W. A. Green and E. Rhian Baylis*

Department of Theoretical Mechanics,

The University,

Nottingham, NG7 2RD, U.K.

Research sponsored by the Air Force Office of Scientific Research,

Air Force Systems Command, USAF under Grant Number AFOSR-86-0330.

The U.S. Government is authorised to reproduce and distribute

reprints for governmental purposes.

* Now at Department of Engineering, University of Leicester,

Leicester, LE1 7RH, U.K.

CONTENTS

1. INTRODUCTION

This paper is concerned with a theoretical and numerical investigation of the propagation of stress waves induced by surface impact on a laminated plate of finite depth and infinite lateral extent. Attention is focussed on the problem of an impulsive line load acting on the upper surface of the plate and generating plane wave disturbances travelling in the laminate along the direction normal to the line load. The plate is constructed of an arrangement of layers (or plies) of fibre-reinforced material in which the reinforcement of each layer is a family of parallel fibres lying in the plane of the layer. The plies are assembled in a periodically repeating configuration of N unit cells, the configuration being defined in terms of the angles between the fibre direction in each ply and some specified reference direction. For the present we have concerned ourselves with a simple 0/90 configuration. Here the unit cell consists of two inner layers, each of thickness h, with the fibres running along the reference direction, and bounded above and below by a layer of thickness h of the same material with fibre direction orthogonal to the reference direction (see Figure 17). This choice of unit cell is made purely for simplicity and the techniques that we use are applicable to any configuration of the unit cell.

We model the fibre reinforced material as a homogeneous continuum of transversely isotropic elastic material with the axis of transverse isotropy along the fibre direction. This means that we look at waves whose wavelengths are an order of magnitude greater than the fibre diameter and inter-fibre spacing so that on the scale of the wavelength the continuum theory might be expected to be valid. Typical of the materials we have in mind is the ICI product PEEK, formed of carbon fibres embedded in a thermoplastic resin, for which typical dimensions are $h \simeq 125\ \mu m$ with the fibre diameter and inter-fibre spacing of the order of $6\ \mu m$. Thus we are thinking in terms of wavelengths of the order of 1/2 to 1/3 the ply thickness or greater for which the non-dimensional wave number $kh = 2\pi h/\Lambda$ (where Λ is the wavelength) varies from zero at infinite wavelength to a value of approximately 18 at $\Lambda = h/3$. For smaller wavelengths, of the order of h/10 or less, the continuum model will break down due to diffraction and scattering by the individual fibres.

There is a considerable simplification in the mathematics to be gained by treating the composite as inextensible in the direction of transverse isotropy. This is an idealization of the fact that the extensional modulus of the continuum along the fibre direction can be of the order of 100 times that in the cross fibre direction. Mathematically, the effect of the idealization is to reduce the order of the differential equations and this leads to solutions involving fewer parameters. A consequence of this reduction in the order of the equations, however, is that it is no longer possible to satisfy all the interface continuity conditions between the plies. This leads to a singular perturbation problem, in which it is necessary to allow the tangential component of traction along the fibre direction to be discontinuous across the interface, with a consequent singularity in the stress component along the fibres, associated with a finite load carried by the surface layer of fibres. This singular perturbation problem has been examined in detail for static problems by Everstine and Pipkin [1] and for dynamic problems by Green [2], Green and Milosavljević [3] and Baylis and Green [4],[5]. In particular, Baylis and Green [4],[5], dealing with a four ply laminate, derive an expression relating the singularity along the fibre direction to the discontinuity in shear stress. They present detailed comparisons of the stresses in the inextensible laminate with those in a strongly anisotropic but not inextensible material. These comparisons show that the inextensible theory provides an acceptable approximation to the stress variation through the laminate except in the very long wavelength region and the dispersion curves for the two material models are also shown to be in good agreement, again with the exception of the very long wavelength limit. As with singular perturbation problems generally, the shear stress discontinuities are to be interpreted in terms of very narrow bands (boundary layers) adjacent to the interfaces, through which there exist high stress gradients, giving large changes in stress across the bands. The associated singular stresses along the boundary fibres are to be interpreted as high stress levels in the boundary layers, which contribute finite loads in the fibre directions when integrated through the boundary layers. It is with these interpretations in mind, that we adopt the idealization of inextensibility to give a mathematically simple model of our fibre reinforced material. Having employed this simplified model to develop and apply

our analytical and numerical techniques, it is proposed in future work to drop the constraint of inextensibility and to employ the full system of governing equations appropriate to the continuum model of the composite as a transversely isotropic elastic material.

In the work reported here, we make no assumptions about the variation of displacements and stresses through the laminate, such as is done in engineering theories of plates and shells. Our method is to solve exactly the system of governing equations appropriate to each layer, matching the solutions across the interfaces and satisfying the appropriate boundary conditions at the upper and lower surfaces of the laminate. This analytical solution is carried out in Section 2 where we work in terms of systems of coupled ordinary differential equations, obtained by taking Laplace transforms in time and Fourier transforms in the in-plane spatial coordinates, of the governing equations of our model. These ordinary differential equations, involving the coordinate normal to the plies as independent variable, are solved using the propagator method of Gilbert and Backus [6], as applied to the inextensible laminate by Green & Baylis [7]. This yields the exact solution for the variation of the transforms with depth throughout the laminate and the approximations arise only in the numerical methods for inverting the transforms.

The problem of inverting the transforms is considered in Section 3. There we show that it is necessary to solve the dispersion equation (relating frequency to wavelength) for plane waves travelling in the plate under traction free boundary conditions at the upper and lower surfaces. Inversion also requires that we evaluate the residue of the inversion integral along each branch of the dispersion equation and we must perform an integration along each branch and a summation over all branches to obtain the solution. In this Section we also briefly outline the stationary phase approximation, which gives the solution at large times. This brings out the role of the group velocity in the asymptotic solution and draws attention to the wave fronts, which are associated with maxima and minima of the group velocity and provide the dominant contributions at large times.

The numerical solution of the dispersion equation and the subsequent numerical integration over the branches of the dispersion curves is outlined in Section 4. It is here that the approximations come into play, since the solutions are necessarily limited to

a finite number of branches and the integrations over each branch must be limited to a finite range of values of the wave number, k. We have chosen as an upper value $k = 20$, corresponding to wavelength of the order of 1/3 the ply thickness but 6 times the fibre diameter and inter-fibre spacing, which we estimate as being the limit at which the continuum model would be valid. We show that restricting the integral to a finite range of values of k gives rise to the phenomenon of "windowing" and we apply the technique due to Hamming [8] in an attempt to reduce this effect.

Section 5, which completes the paper, contains detailed results in graphical form and some discussion of the contribution of the higher harmonics as compared with the first two modes. The results consist of graphs of the dispersion equations, which illustrate the plateau and step regions arising in the higher harmonics and of the corresponding group velocity curves, which display the contributions of the high harmonics to the wave front disturbance at large times. Graphs are also presented which show the variation of displacements and stresses, at the upper and lower surfaces and on the middle plane, as functions of position at various times.

2. GOVERNING EQUATIONS AND PROPAGATOR SOLUTIONS

We consider a laminated plate composed of layers of the idealized fibre reinforced material which is inextensible in the fibre direction, the fibres being in the plane of the layers and with the fibre directions in adjacent layers being orthogonal to each other. We choose a Cartesian Coordinate system of axes with origin in the middle surface of one of the layers and with Ox_3 parallel to the fibre direction in that layer. Letting Ox_2 be parallel to the fibre direction in the adjacent layers then the normal to the laminate coincides with the x_1-axis. We shall be concerned with plane waves generated by a line load acting on the upper surface of the laminate along a line making an angle $(\pi/2-\gamma)$ with the x_3-axis. The resulting disturbance will generate a displacement vector $\underline{u}(x_1,x_2,x_3,t)$ of the form

$$\underline{u}(x_1,x_2,x_3,t) = \underline{u}(x_1,x,t) \ , \tag{1}$$

where

$$x = x_3 \cos\gamma + x_2 \sin\gamma \ , \tag{2}$$

which corresponds to a plane wave whose normal lies in the x_2x_3 plane at an angle $-\gamma$ to the x_3-axis (see Figure 18). The components $t_{ij}(x_1,x_2,x_3,t)$ of stress in each layer of the laminate will likewise reduce to functions $t_{ij}(x_1,x,t)$ and these are given in terms of the strain components via the constitutive equations appropriate to each layer (see for example Baylis & Green [4]). Before proceeding further it is convenient to take the Laplace Transform in time and Fourier Transform with respect to the space variable x of both the displacement components $u_i(x_1,x,t)$ and the stress components $t_{ij}(x_1,x,t)$. Thus we define dispacement transforms U,V,W by

$$\begin{aligned} U(x_1,k,\hat{s}) &= \int_{-\infty}^{\infty}\int_0^{\infty} u_1(x_1,x,t)e^{-\hat{s}t}e^{-ikx}\,dt\,dx \ , \\ V(x_1,k,\hat{s}) &= \int_{-\infty}^{\infty}\int_0^{\infty} u_2(x_1,x,t)e^{-\hat{s}t}e^{-ikx}\,dt\,dx \ , \\ W(x_1,k,\hat{s}) &= \int_{-\infty}^{\infty}\int_0^{\infty} u_3(x_1,x,t)e^{-\hat{s}t}e^{-ikx}\,dt\,dx, \end{aligned} \tag{3}$$

and stress transforms $T_{ij}(x_1,k,\hat{s})$ by

$$T_{ij}(x_1,k,\hat{s}) = \int_{-\infty}^{\infty}\int_{0}^{\infty} t_{ij}(x_1,x,t)e^{-\hat{s}t}e^{-ikx}\,dt\,dx\ . \tag{4}$$

In a general elastic material the transforms of the constitutive equations and the stress equations of motion then yield a system of six first order ordinary differential equations for $U,V,W,T_{11},T_{12},T_{13}$, as functions of x_1, together with three equations to determine the remaining stress transforms T_{22},T_{23},T_{33} in terms of these six quantities. For the idealized inextensible material, however, the displacement transform in the fibre direction is identically zero and the reaction stress associated with the inextensibility constraint is not determined by the constitutive equations but is obtained from one of the stress equations of motion. Thus the equations reduce to four first order ordinary differential equations together with relations to determine the remaining stress transforms. Using the subscript 1 to denote the layers for which the fibre direction is parallel to the x_3-axis, the appropriate equations may be derived from those given in Baylis & Green [4]. The differential equations then have the form

$$\begin{aligned}
\frac{dU_1}{dx_1} &= \frac{c_2^2}{c_1^2}T_1 - \left[1 - \frac{2c_2^2}{c_1^2}\right]iks\,V_1\ ,\\
\frac{dV_1}{dx_1} &= S_1 - iks\,U_1\ ,\\
\frac{dT_1}{dx_1} &= \frac{(\hat{s}^2-k^2c^2c_3^2)}{c_2^2}U_1 - iks\,S_1\ ,\\
\frac{dS_1}{dx_1} &= \left[4k^2s^2\left[1 - \frac{c_2^2}{c_1^2}\right] + \frac{k^2c^2c_3^2 + \hat{s}^2}{c_1^2}\right]V_1 - iks\left[1 - \frac{2c_2^2}{c_1^2}\right]T_1\ ,
\end{aligned} \tag{5}$$

where $T_1 = \frac{T_{11}}{\rho c_2^2}$, $S_1 = \frac{T_{12}}{\rho c_2^2}$, $c = \cos\gamma$ and $s = \sin\gamma$.

The inextensibility constraint becomes

$$W_1 = 0\ , \tag{6}$$

and the stress transforms are given by

$$T_{22} = \rho(c_1^2-2c_2^2)\frac{c_2^2}{c_1^2}T_1 + iks\rho^4c_2^2\left[1-\frac{c_2^2}{c_1^2}\right]V_1 ,$$

$$T_{23} = \rho c_3^2 ikc\, V_1 , \qquad T_{31} = \rho c_3^2 ikc\, U_1 , \tag{7}$$

$$T_{33} = -\rho\frac{c_3^2c_2^2}{c_1^2}(T_1 + 2iks\, V_1) .$$

In equations (5) and (7), ρ is the density of the continuum and c_1^2, c_2^2, c_3^2 are squared wave speeds derived from the elastic constants of the continuum (Green [2]).

The solution of the differential equations (4) may be written in terms of the propagator matrix $\underset{\sim}{P}(x_1-\bar{x}_1)$ in the form

$$\underset{\sim}{Y}(x_1) = \underset{\sim}{P}(x_1-\bar{x}_1)\underset{\sim}{Y}(\bar{x}_1) , \tag{8}$$

where $\bar{x}_1$ is some fixed value of x_1 within the layer and x_1 is any other value in the same layer, $\underset{\sim}{Y}(x_1)$ is the vector $(T_1(x_1), S_1(x_1), U_1(x_1), V_1(x_1))^T$ where T denotes the transpose, and the components of the 4 × 4 matrix $\underset{\sim}{P}$ are given in Table 1, page 33.

Using subscript 2 to denote the transformed quantities within a layer of material with the fibre direction parallel to the x_2–axis, the constraint condition gives

$$V_2 = 0 , \tag{9}$$

and the equations equivalent to (5) involve U_2, W_2, T_2 and R_2 where $R_2 = T_{13}/\rho c_2^2$. Letting $\underset{\sim}{Z}(x_1)$ denote the vector $(T_2, R_2, U_2, W_2)^T$ the solution of these equations is given by

$$\underset{\sim}{Z}(x_1) = \underset{\sim}{Q}(x_1-\hat{x}_1)\underset{\sim}{Z}(\hat{x}_1) \tag{10}$$

where $\hat{x}_1$ is some fixed value of x_1 within the layer and x_1 is any other value in the same layer. The components of the 4 × 4 propagator matrix $\underset{\sim}{Q}$ may be derived from those of $\underset{\sim}{P}$ by the substitutions given in Table 2, page 33.

Equations (8) and (10) yield the solution of the governing equations in individual layers of material with fibres parallel to the x_3–axis and the x_2–axis respectively. In order to obtain the solution in a multi-layered laminate it is necessary to satisfy the appropriate conditions at the upper and lower surfaces as well as continuity conditions at the interfaces. In general, the conditions at the interface between two dissimilar elastic materials which are bonded together requires continuity of all three displacement

components and the three components of traction across the interface. In terms of the transformed quantities these continuity conditions are

$$U_1 = U_2, \quad V_1 = V_2, \quad W_1 = W_2,$$
$$T_1 = T_2 \quad S_1 = S_2, \quad R_1 = R_2 \tag{11}$$

For the idealized inextensible material, however, it has been shown by Baylis and Green [4] that there exists the possibility of a discontinuity in the tangential component of stress parallel to the fibre direction across any surface in the material and in particular this allows a discontinuity in S in material 2 at any interface or free boundary in these materials. Thus at an interface between materials 1 and 2 conditions (11) reduce to

$$U_1 = U_2, \quad T_1 = T_2, \quad V_1 = V_2, \quad W_1 = W_2 \tag{12}$$

the last two conditions being a consequence of the inextensibility constraints applied to the displacement continuity conditions.

Consider now a layer of thickness $2h$ of material 1 sandwiched between two layers of material 2. Letting Y^L and Y^U denote the value of the vector Y at the bottom and top of this layer respectively we have from equation (8) that

$$Y^U = P(2h)Y^L = P(h)P(h)Y^L \tag{13}$$

where we have made use of the property that for any propagator matrix $P(a+b) = P(a)P(b)$ (see Gilbert & Backus [6]). If we now impose the condition that $V_1^U = 0$, $V_1^L = 0$, arising from the interface conditions (12), it is possible to eliminate the (discontinuous) stresses S^U, S^L from equations (13) to obtain

$$\underset{\sim}{X}_1^U = \frac{\underset{\sim}{R}\,\hat{\underset{\sim}{R}}}{\det \underset{\sim}{R}}\,\underset{\sim}{X}_1^L \tag{14}$$

where

$$\underset{\sim}{X}_1 = \begin{bmatrix} T_1 \\ U_1 \end{bmatrix}, \quad \underset{\sim}{R} = \begin{bmatrix} r_{11} & r_{12} \\ r_{21} & r_{22} \end{bmatrix}, \quad \hat{\underset{\sim}{R}} = \begin{bmatrix} r_{22} & r_{12} \\ r_{21} & r_{11} \end{bmatrix} \tag{15}$$

and the components r_{ij} of $\underset{\sim}{R}$ are given in terms of the components p_{ij} of $\underset{\sim}{P}(h)$ by the expressions

$$r_{11} = p_{11} - \frac{p_{14}p_{41}}{p_{44}}, \quad r_{12} = p_{13} - \frac{p_{12}p_{43}}{p_{42}},$$
$$r_{21} = p_{31} - \frac{p_{34}p_{41}}{p_{44}}, \quad r_{22} = p_{33} - \frac{p_{32}p_{43}}{p_{42}}. \tag{16}$$

In the same way, if we consider a layer of thickness 2h of material 2 sandwiched between layers of material 1 we may express the value of $\underset{\sim}{X}_2$ at the top of the layer in terms of the value at the bottom in the form

$$\underset{\sim}{X}_2^u = \frac{\underset{\sim}{F}\,\hat{\underset{\sim}{F}}}{\det \underset{\sim}{F}}\,\underset{\sim}{X}_2^L \tag{17}$$

where

$$\underset{\sim}{X}_2 = \begin{bmatrix} T_2 \\ U_2 \end{bmatrix}, \quad \underset{\sim}{F} = \begin{bmatrix} f_{11} & f_{12} \\ f_{21} & f_{22} \end{bmatrix}, \quad \hat{\underset{\sim}{F}} = \begin{bmatrix} f_{22} & f_{12} \\ f_{21} & f_{11} \end{bmatrix} \tag{18}$$

and the components f_{ij} of $\underset{\sim}{F}$ are related to the components $q_{\ell m}$ of $\underset{\sim}{Q}(h)$ by equations analogous to (16) above. Using the first two of the continuity conditions (12) to relate $\underset{\sim}{X}_2$ at the top of one layer to $\underset{\sim}{X}_1$ at the bottom of the next and applying (17) and (14) gives the relation

$$\underset{\sim}{X}^{(\alpha+1)} = \frac{(\underset{\sim}{R}\,\hat{\underset{\sim}{R}})}{\det \underset{\sim}{R}}\,\frac{(\underset{\sim}{F}\,\hat{\underset{\sim}{F}})}{\det \underset{\sim}{F}}\,\underset{\sim}{X}^{(\alpha)} \ . \tag{19}$$

This gives the vector $\underset{\sim}{X}^{(\alpha+1)}$ at the top of unit cell $(\alpha+1)$ in terms of the vector $\underset{\sim}{X}^{\alpha}$ at the top of unit cell α where the unit cell is a layer of depth 2h of material 1 on top of a layer of depth 2h of material 2 embedded in a repeating pattern. It is possible to show that (19) is equivalent to either of the relations

$$\begin{aligned} \underset{\sim}{X}^{(\beta+1)} &= \frac{\hat{\underset{\sim}{F}}\,\underset{\sim}{R}\,\hat{\underset{\sim}{R}}\,\underset{\sim}{F}}{\det \underset{\sim}{R}\,\det \underset{\sim}{F}}\,\underset{\sim}{X}^{(\beta)} \ , \\ \underset{\sim}{X}^{(\gamma+1)} &= \frac{\hat{\underset{\sim}{R}}\,\underset{\sim}{F}\,\hat{\underset{\sim}{F}}\,\underset{\sim}{R}}{\det \underset{\sim}{R}\,\det \underset{\sim}{F}}\,\underset{\sim}{X}^{(\gamma)} \ . \end{aligned} \tag{20}$$

The first of these expressions is appropriate to a unit cell consisting of a layer 2h of material 1 sandwiched above and below by a layer of depth h of material 2 and embedded in a repeating pattern and the second of equations (20) refers to a layer of depth 2h of material 2 between two layers of material 1 each of thickness h forming a unit cell in a repeating pattern.

We shall adopt the first version given in equation (20) and write

$$\underset{\sim}{X}^{(\beta+1)} = \frac{\hat{\underset{\sim}{F}}\,\underset{\sim}{R}\,\hat{\underset{\sim}{R}}\,\underset{\sim}{F}}{\det \underset{\sim}{R}\,\det \underset{\sim}{F}}\,\underset{\sim}{X}^{(\beta)} = \frac{\underset{\sim}{C}\,\hat{\underset{\sim}{C}}}{\det \underset{\sim}{C}}\,\underset{\sim}{X}^{(\beta)} = \underset{\sim}{D}\,\underset{\sim}{X}^{(\beta)} \ , \tag{21}$$

where

$$\underset{\sim}{C} = \hat{\underset{\sim}{F}}\,\underset{\sim}{R}, \quad \hat{\underset{\sim}{C}} = \hat{\underset{\sim}{R}}\,\underset{\sim}{F} \quad \text{and} \quad \underset{\sim}{D} = \frac{\underset{\sim}{C}\,\hat{\underset{\sim}{C}}}{\det \underset{\sim}{C}} \ . \tag{22}$$

Applying equation (21) to a sequence of (n−1) unit cells then gives

$$\underset{\sim}{X}^{(n-\frac{1}{2})} = \underset{\sim}{D}^{(n-1)}\ \underset{\sim}{X}^{(\frac{1}{2})}$$

$$= \frac{(\lambda_1^{n-1}-\lambda_2^{n-1})\underset{\sim}{D}\ \underset{\sim}{X}^{(\frac{1}{2})} - \lambda_1\lambda_2(\lambda_1^{n-2}-\lambda_2^{n-2})\underset{\sim}{X}^{(\frac{1}{2})}}{(\lambda_1-\lambda_2)} \quad , \tag{23}$$

where we have used the Cayley-Hamilton theorem to express $\underset{\sim}{D}^{n-1}$ in terms of $\underset{\sim}{D}$, $\underset{\sim}{I}$ and the eigenvalues λ_1, λ_2 of $\underset{\sim}{D}$. Equation (23) refers to a set of (n-1) unit cells assumed to be embedded in a repeating pattern so that the constraint conditions arising from inextensibility is operative on every layer of thickness 2h of both material *1* and material *2*. In order to consider wave motion in a laminate of finite depth 2nh, it is necessary to encase the (n-1) unit cells in two half cells, each consisting of an inner layer of material *2* and an outer layer of material *1*. Then each of the layers of material *2* is still constrained by the inextensibility condition imposed by the outer layer of material *1* and the expressions previously derived for the transmission through material *2* may be employed at the top and the bottom of the (n-1) cells to give

$$\underset{\sim}{X}^{(n-\frac{1}{2})} = \left[\underset{\sim}{F}\ \underset{\sim}{D}^{n-1} - \frac{\hat{\underset{\sim}{F}}}{\det\ \underset{\sim}{F}}\right]\underset{\sim}{X}^{(\frac{1}{2})} \quad . \tag{24}$$

Each of the outer layers (of thickness h) of material *1* at the top and bottom of the complete plate must be treated separately. Each is subject to the constraint $V_1 = 0$ at the interface with material *2* and it will be assumed that the tangential component of traction S_1 vanishes at the outer surface. Applying equation (8) to the layer on the upper surface of the plate gives

$$\underset{\sim}{Y}(h) = \underset{\sim}{P}(h)\underset{\sim}{Y}(0), \tag{25}$$

and making use of the conditions $S_1(h) = 0$ and $V_1(0) = 0$ allows the values of $T_1(h)$, $U_1(h)$ to be given in terms of $T_1(0)$, $U_1(0)$ by the expression

$$\underset{\sim}{X}_1(h) = \underset{\sim}{S}\underset{\sim}{X}_1(0) \quad , \tag{26}$$

where the elements of the 2×2 matrix $\underset{\sim}{S}$ are given in terms of the elements p_{ij} of $\underset{\sim}{P}(h)$ by

$$\begin{aligned} s_{11} &= p_{11} - \frac{p_{12}p_{21}}{p_{22}} \quad , & s_{12} &= p_{13} - \frac{p_{12}p_{23}}{p_{22}} \quad , \\ s_{21} &= p_{31} - \frac{p_{32}p_{21}}{p_{22}} \quad , & s_{22} &= p_{33} - \frac{p_{32}p_{23}}{p_{22}} \quad . \end{aligned} \tag{27}$$

Applying the same procedure to the layer on the bottom surface of the plate leads to the expression

$$\underset{\sim}{X}_1(h) = \hat{\underset{\sim}{S}}\ \underset{\sim}{X}_1(0) = \frac{\hat{\underset{\sim}{S}}}{\det\ \underset{\sim}{S}}\ \underset{\sim}{X}_1(0) \tag{28}$$

where

$$\hat{S} = \begin{bmatrix} s_{22} & s_{12} \\ s_{21} & s_{11} \end{bmatrix}, \tag{29}$$

and the last expression in equation (28) uses the result that det $\underset{\sim}{S} = 1$. Combining (24) with (26) and (28) gives for the overall laminate

$$\begin{aligned} \underset{\sim}{X}^{(n)} &= \underset{\sim}{S}\ \underset{\sim}{F}\ \underset{\sim}{D}^{n-1}\ \frac{\hat{\underset{\sim}{F}}\ \hat{\underset{\sim}{S}}}{\det\ \underset{\sim}{F}\ \underset{\sim}{S}}\ \underset{\sim}{X}^{(0)} \\ &= \underset{\sim}{M}\ \underset{\sim}{X}^{(0)} \end{aligned} \tag{30}$$

where $\underset{\sim}{X}^{(0)}$ and $\underset{\sim}{X}^{(n)}$ denote the value of $\underset{\sim}{X}$ at the bottom surface and the top surface respectively and $\underset{\sim}{M}$ is the overall transmission matrix for the laminate. If the upper surface of the laminate is subjected to a time dependent normal line load of the form

$$t_{11}(x_2,x_3,t) = P(t)\ \delta(x_3 \cos\gamma + x_1 \sin\gamma) = P(t)\ \delta(x)$$

where $\delta(x)$ is the Dirac delta function, and the lower surface of the laminate is traction free, then

$$\underset{\sim}{X}^{(n)} = \begin{bmatrix} \bar{P}(\hat{s}) \\ U_1^{(n)} \end{bmatrix}, \qquad \underset{\sim}{X}^{(0)} = \begin{bmatrix} 0 \\ U_1^{(0)} \end{bmatrix}, \tag{31}$$

where $\bar{P}(\hat{s})$ is the Laplace transform of P(t). Substituting from (31) into (30) then gives the displacement transform $U_1^{(0)}$ at the bottom surface in terms of the stress transform $\bar{P}(\hat{s})$ as

$$U_1^{(0)} = \frac{\bar{P}(\hat{s})}{m_{12}(k,\hat{s})}, \tag{32}$$

and the displacement transform $U_1^{(n)}$ at the bottom surface is given by

$$U_1^{(n)} = \frac{m_{22}(k,\hat{s})}{m_{12}(k,\hat{s})}\ \bar{P}(\hat{s}). \tag{33}$$

Equations (32) and (33) relate to the normal line load acting on the upper surface of the plate. We may examine the case of a tangential line load in a similar fashion. Because of the inextensibility constraint in the x_3-direction at the upper surface the component t_{13} of the tangential stress in the x_3-direction induces a singularity in the

stress component t_{33} at the surface but transmits no disturbance into the material. It is only the tangential component t_{12} in the x_2-direction that produces a wave motion in the underlying laminate. To obtain the solution to this problem we return to equation (24). This relates the vector $\underset{\sim}{X}^{(\frac{1}{2})}$ at the interface between the bottom layer of material *1* and the rest of the laminate to the vector $\underset{\sim}{X}^{(n-\frac{1}{2})}$ at the interface between the laminate and the top layer of material *1*. To complete the solution we now use equation (25) as before but the conditions imposed on each of the outer layers of material *1* are that $V_1 = 0$ at the interface of the layer with material *2* and that $T_1 = 0$ at the outer boundary. This allows us to express the vector $\hat{\underset{\sim}{X}}^u = (S_1\ U_1)^T$ at the upper surface of the top layer in terms of the vector $\underset{\sim}{X}^L = (T_1\ U_1)^T$ between the top layer and the rest of the plate in the form

$$\hat{\underset{\sim}{X}} = \underset{\sim}{G}\ \underset{\sim}{X}^L\ , \tag{34}$$

where the elements of the matrix $\underset{\sim}{G}$ are given by

$$\begin{aligned} g_{11} &= p_{21} - \frac{p_{11}p_{22}}{p_{12}}\ , \qquad & g_{12} &= p_{23} - \frac{p_{13}p_{22}}{p_{12}}\ , \\ g_{21} &= p_{31} - \frac{p_{11}p_{32}}{p_{12}}\ , \qquad & g_{22} &= p_{33} - \frac{p_{13}p_{32}}{p_{12}}\ . \end{aligned} \tag{35}$$

Combining equation (34) and its equivalent at the bottom layer of the laminate, with equation (24) then yields

$$\hat{\underset{\sim}{X}}(n) = \left[\underset{\sim}{G}\ \underset{\sim}{F}\ \underset{\sim}{D}^{n-1}\ \frac{\hat{\underset{\sim}{F}}\ \hat{\underset{\sim}{G}}}{\det \hat{\underset{\sim}{F}}\ \hat{\underset{\sim}{G}}}\right] \hat{\underset{\sim}{X}}(0)\ , \tag{36}$$

where

$$\hat{G} = \begin{bmatrix} g_{22} & g_{12} \\ g_{22} & g_{11} \end{bmatrix}\ , \tag{37}$$

and $$\det G = g_{11}g_{22} - g_{21}g_{12} = -\ p_{22}/p_{12}. \tag{38}$$

In terms of the overall matrix $\underset{\sim}{M}$ defined by equation (30) we may write equation (36) in the form

$$\hat{\underset{\sim}{X}}(n) = \left[\underset{\sim}{G}\ \underset{\sim}{S}^{-1}\ \underset{\sim}{M}\ \frac{\hat{\underset{\sim}{S}}^{-1}\ \hat{\underset{\sim}{G}}}{\det \hat{\underset{\sim}{G}}}\right] \hat{\underset{\sim}{X}}(0) = \underset{\sim}{N}\ \hat{\underset{\sim}{X}}(0)\ . \tag{39}$$

For a tangential line load with component t_{12} given by

$$t_{12}(x_2,x_3,t) = Q(t)\ \delta(x_3 \cos\gamma + x_2 \sin\gamma) = Q(t)\ \delta(x) \tag{40}$$

acting on the upper surface of the plate and with the lower surface traction free, equation (39) gives

$$U_1^{(0)} = \frac{\bar{Q}(\hat{s})}{n_{12}(k,\hat{s})}$$
$$U_1^{(n)} = \frac{n_{22}(k,\hat{s})\bar{Q}(\hat{s})}{n_{12}(k,\hat{s})} \tag{41}$$

where $\bar{Q}(\hat{s})$ is the Laplace transform of Q(t) and $U_1^{(0)}$, $U_1^{(n)}$ are the transforms of the normal displacements on the lower and upper surfaces respectively. Using the expressions for the components of $\underset{\sim}{G}$ and $\underset{\sim}{S}$ given in equation (35) and (27) the components n_{12} and n_{22} of the matrix $\underset{\sim}{N}$ may be expressed in terms of the components of $\underset{\sim}{M}$ and the propagator $\underset{\sim}{P}(h)$ in the form

$$n_{12} = -\frac{p_{22}m_{12}}{p_{12}} \quad , \quad n_{22} = m_{22} - \frac{p_{32}m_{12}}{p_{12}} \quad . \tag{42}$$

Combining equations (41) linearly with (32) and (33) gives the solution for an arbitrary line load on the upper surface of the plate.

Equation (33) gives the transform of the normal component of displacement at the upper surface due to the specified normal line load. From the propagator solution (8) and equations (7) it is possible to obtain expressions for the transform of the tangential displacement $V_1^{(n)}$ at the upper surface and the transformed components of stress. These are given by

$$V_1^{(n)} = \frac{p_{43}U_1^{(n)} - p_{41}\bar{P}(\hat{s})}{p_{44}} \quad , \quad (p_{44} \neq 0)$$
$$T_{22}^{(n)} = \rho c_2^2\left\{\left[1 - \frac{2c_2^2}{c_1^2}\right]\bar{P}(\hat{s}) + iks\left[1 - \frac{c_2^2}{c_1^2}\right]V_1^{(n)}\right\} ,$$
$$T_{23}^{(n)} = \rho c_3^2 ikcV_1^{(n)} \quad , \quad T_{13}^{(n)} = \rho c_3^2 ikcU_1^{(n)} \quad , \tag{43}$$
$$T_{33}^{(n)} = -\rho c_3^2\left\{\frac{c_2^2}{c_1^2}\left[\bar{P}(\hat{s}) + 2iksV_1^{(n)}\right] - U_1^{(n)}\delta(x_1 - 2nh)\right\} .$$

In equation (43) the component $T_{13}^{(n)}$ relates to the limiting value on approaching the surface from within the material and this stress component jumps discontinuously to zero on crossing the surface. The Dirac delta function term in the expression for $T_{33}^{(n)}$ gives the singularity in the reaction stress along the fibres in the surface, which is required in order to balance the shear stress discontinuity. (In the argument of the delta function,

the origin of coordinates has been taken to be in the middle surface of the 2n ply laminate.) Results appropriate to the lower surface of the laminate may be derived from equations (43) on replacing $U_1^{(n)}$ by $U_1^{(0)}$, $V_1^{(n)}$ by $V_1^{(0)}$ and suppressing all the terms involving $\bar{P}(\hat{s})$.

Using the propagator solutions, together with equations (7) and their equivalents in material *2*, it is possible to derive the displacement and stress transforms at any value of x_1 throughout the laminate. As an illustration of the application of these methods we calculate the transforms of both displacements and stresses at the interface between the top layer of material *1* and the remainder of the laminate. The propagator solution is

$$\underline{X}^{(n-\frac{1}{2})} = \underline{S}^{-1}\,\underline{X}^{(n)} \ , \tag{44}$$

which, on using equations (31) and (33) gives T_1 and U_1 at the interface as

$$\begin{aligned} T_1 &= \left[s_{22} - \frac{s_{12}m_{22}}{m_{12}}\right]\bar{P}(\hat{s}) \ , \\ U_1 &= -\left[s_{21} - \frac{s_{11}m_{22}}{m_{12}}\right]\bar{P}(\hat{s}) \ . \end{aligned} \tag{45}$$

Then the interface continuity conditions give $T_2 = T_1$, $U_2 = U_1$, together with $V_1 = V_2 = 0$ and $W_1 = W_2 = 0$. The tangential components of traction in material *1* at the interface are then given by

$$\begin{aligned} T_{12}^{(1)} &= \rho c_2^2 S_1 = -\rho c_2^2\left[\frac{p_{21}T_1 + p_{23}U_1}{p_{22}}\right], \qquad (p_{22} \neq 0) \\ T_{13}^{(1)} &= \rho c_3^2 ikcU_1 \ , \end{aligned} \tag{46}$$

and the corresponding components in material *2* are

$$\begin{aligned} T_{12}^{(2)} &= \rho c_3^2 iksU_1 \ , \\ T_{13}^{(2)} &= \rho c_2^2 R_2 = \rho c_2^2\left[\frac{q_{41}T_1 - q_{43}U_1}{q_{42}}\right], \qquad (q_{42} \neq 0) \ . \end{aligned} \tag{47}$$

The discontinuities in these traction components across the interface are balanced by singularities at the interface along the fibre direction in each material and combining these with the results derived from equations (7) and their equivalents gives the in-plane stress components in the two materials. The results are

$$T_{22}^{(1)} = \rho c_2^2\left[1 - \frac{2c_2^2}{c_2^2}\right]T_1, \quad T_{23}^{(1)} = 0, \quad T_{33}^{(1)} = \frac{\rho c_3^2 c_2^2}{c_1^2} T_1 - \left[\frac{T_{13}^{(1)} - T_{13}^{(2)}}{ikc}\right]\delta(x^*),$$

$$T_{22}^{(2)} = -\frac{\rho c_3^2 c_2^2}{c_1^2} T_1 - \left[\frac{T_{12}^{(1)} - T_{12}^{(2)}}{iks}\right]\delta(x^*), \quad T_{23}^{(2)} = 0, \quad T_{33}^{(2)} = \rho c_2^2\left[1 - \frac{2c_2^2}{c_1^2}\right]T_1, \tag{48}$$

where the argument of the δ function is $x^* = x-(2n-1)h$, corresponding to the origin at the middle surface of the laminate. Results similar to those detailed in equations (45) - (48) may be obtained at any other interface of the laminate whilst at any interior point in any layer it is possible to also determine the non-zero in-plane displacement (V_1 or W_2). In the next section we consider the problem of inverting these transforms to give the required solutions.

3. TRANSFORM INVERSION

The techniques developed in Section 2 yield the transforms of the displacements and stresses throughout the laminate as known functions of the transform parameters k and $\hat{s}$ at any value of x_1. In order to determine the displacements and stresses as functions of the coordinate $x = x_3 \cos\gamma + x_2 \sin\gamma$, normal to the line load and of the time t, it is necessary to invert these transforms. Typical of the quantities to be considered is the transform of the normal displacement at the upper surface due to a normal line load, which is given by equation (33) in the form

$$U_1^{(n)} = \frac{m_{22}(k,\hat{s})}{m_{12}(k,\hat{s})} \bar{P}(\hat{s}) \quad . \tag{33}$$

Letting $u_1(2nh,x,t)$ denote the normal displacement on the upper surface $x_1 = 2nh$, due to a line load which consists of a unit delta function in time $P(t) = \delta(t)$, for which $\bar{P}(\hat{s}) = 1$, the displacement $u_1^P(x,t)$ corresponding to the transform (33) associated with any P(t) is then given as the convolution of P(t) with $u_1(2nh,x,t)$ in the form

$$u_1^P(x,t) = \int_0^t u_1(2nh,x,\tau)P(t-\tau)\, d\tau \, . \tag{49}$$

Accordingly we restrict attention to inverting the transform (33) with $\bar{P}(\hat{s}) = 1$, for which the formal solution is

$$u_1(2nh,x,t) = \frac{1}{4\pi^2 i} \int_{-\infty}^{\infty} \int_{\gamma-i\infty}^{\gamma+i\infty} \frac{m_{22}(k,\hat{s})}{m_{12}(k,\hat{s})} e^{\hat{s}t} e^{ikx} \, d\hat{s} \, dk \, . \tag{50}$$

The integral with respect to $\hat{s}$ may be evaluated in terms of the residues of the integrand at the zeros of the function $m_{12}(k,\hat{s})$ in the left half plane. The equation

$$m_{12}(k, i\omega) = 0 \tag{51}$$

is the dispersion equation for plane wave propagation in the laminate, corresponding to waves travelling in the direction of the normal to the line load under traction free conditions at the two surfaces of the plate. This equation has an infinite number of pairs of roots, $\omega_j = \pm\omega_j(k)$ $(j=1,2,\ldots)$, each pair corresponding to forward and backward travelling waves associated with one branch of the dispersion curve. In terms of these solutions, equation (49) becomes

$$u_1(2nh,x,t) = \frac{1}{2\pi} \int_{-\infty}^{\infty} dk \sum_{j=1}^{\infty} \left\{ \frac{m_{22}(k,\hat{s})}{dm_{12}/d\hat{s}} e^{i(kx-i\hat{s}t)} \right\}_{\hat{s} = \pm i\omega_j(k)} . \tag{52}$$

Both $m_{12}(k,\hat{s})$ and $m_{22}(k,\hat{s})$ are even functions of $\hat{s}$ and equation (52) may be written as

$$u_1(2nh,x,t) = \frac{i}{\pi} \sum_{j=1}^{\infty} \int_{-\infty}^{\infty} R_j(k) \sin \omega_j(k)t \, e^{ikx} \, dk \tag{53}$$

where

$$R_j(k) = \left[\frac{m_{22}(k,\hat{s})}{dm_{12}/d\hat{s}}\right]_{\hat{s} = +i\omega_j(k)} = -\left[\frac{m_{22}(k,\hat{s})}{dm_{12}/d\hat{s}}\right]_{\hat{s} = -i\omega_j(k)} . \tag{54}$$

It may also be shown that $R_j(k)$ is an even function of k and equation (53) may be further simplified to give

$$u_1(2nh,x,t) = \frac{2i}{\pi} \sum_{j=1}^{\infty} \int_{0}^{\infty} R_j(k) \sin \omega_j(k)t \cos kx \, dk$$

Equation (43) contains an expression for $V_1^{(n)}$ which is valid provided $p_{44} \neq 0$ and which therefore has the same singularities as $U_1^{(n)}$ for the case $\bar{P}(\hat{s}) = 1$. It may be shown that p_{43}/p_{44} is an odd function of k and we may therefore express the tangential displacement $v_1(2nh,x,t)$ associated with a unit delta function normal line load as

$$v_1(2nh,x,t) = -\frac{2}{\pi} \sum_{j=1}^{\infty} \int_{0}^{\infty} h_j(k) R_j(k) \sin \omega_j(k)t \sin kx \, dk ,$$

where $h_j(k)$ is the value of the ratio p_{43}/p_{44} evaluated at $\hat{s} = i\omega_j(k)$.
The formulae for the transforms of the stress components in equation (43) involve terms of the form $ikU_1^{(n)}$ and $ikV_1^{(n)}$ and these when inverted give $du_1(2nh,x,t)/dx$ and $dv_1(2nh,x,t)/dx$ respectively.

Equations (45) give the transformed normal displacement and normal component of traction at the interface between the top surface layer of material *1* and the rest of the laminate. These have the same singularities as the expression (33) and their inverses yield

$$u_1\left[(2n-1)h,x,t\right] = \frac{2i}{\pi} \sum_{j=1}^{\infty} \int_{0}^{\infty} s_{11}(k) R_j(k) \sin \omega_j(k)t \cos kx \, dk,$$

$$t_{11}\left[(2n-1)h,x,t\right] = -\frac{2}{\pi} \sum_{j=1}^{\infty} \int_{0}^{\infty} s_{12}(k) R_j(k) \sin \omega_j(k)t \sin kx \, dk, \tag{55}$$

where we have used the fact that $s_{11}(k)$ is an even function of k and $s_{12}(k)$ an odd function of k. Equations (46), (47) and (48) then yield the remaining stress components

on the two sides of the interface in a similar fashion, the resulting integrals being of the forms given in equations (55) but with different factors multiplying $R_j(k)$.

All the results derived in this section relate to the problem of the normal line load acting on the upper surface of the laminate. Results for the effect of the tangential line load may be obtained in a completely analagous way by starting with the solutions given in equations (41) rather than using the solutions (33). Referring to equations (42), it may be seen that the zeros of the element n_{12}, which determine the singularities of the transforms, occur at the zeros of m_{12} and possibly at the zeros of p_{22}. A detailed examination of the product $p_{22}m_{12}$ shows, however, that this does not vanish at the zeros of p_{22} and therefore the singularities of these transforms occur on the same dispersion curves as for the normal line load problem. Thus all the inversion integrals associated with the tangential line load problem involve the residues $R_j(k)$ multiplied by some appropriate factor. Hence for both the normal and tangential line loads the problem of inverting the transforms reduces to evaluating an infinite sum of infinite integrals of the form

$$\sum_{j=1}^{\infty} \int_0^{\infty} f_j(k) R_j(k) \sin \omega_j(k) t \begin{Bmatrix} \sin kx \\ \cos kx \end{Bmatrix} dk \qquad (56)$$

where $f_j(k)$ is some factor arising from a function of k and $\hat{s}$ which is evaluated on the branch $\hat{s} = i\omega_j(k)$ of the dispersion curve.

The expression (56) consists of a sum of integrals, one along each branch of the dispersion curve. In general both the integration and summation have to be carried out numerically and we must therefore limit the range of integration to some finite interval $(0,\hat{k})$ and restrict the summation to a finite number of branches $j=1,\ldots,P$ of the dispersion curve. We then have to construct a computer programme to solve the dispersion equation

$$m_{1,2}(k, i\omega_j) = 0 \qquad (57)$$

numerically in order to obtain values of $\omega_j(k)$ along each of the P branches for values of k taken at M intervals $\Delta k = \hat{k}/M$ from $k=0$ to $k=\hat{k}$. It is also necessary to evaluate the residues $R_j(k)$ at each of these values of k for each of the branches $j=1,2,\ldots P$.

An alternative approximate solution, valid for large times, may be derived by the

method of stationary phase. Writing the integrals which appear in equation (52) in the form

$$\int_{-\infty}^{\infty} R_j(k)\ e^{i(kx-\omega_j t)}\ dk = \int_{-\infty}^{\infty} R_j(k)\ e^{-it\theta_j}\ dk\ ,$$

where

$$\theta_j = (\omega_j(k) - k\ x/t),$$

the rapid oscillation produced by the exponential term for small changes in k (and therefore θ_j) at large values of t produces cancellation of the integrands, except for those values of k for which $d\theta_j/dk$ is zero. The major contribution to the integral then comes at those values k_g of k for which θ_j is stationary and which are given by solving the equation

$$C_j(k_g) = x/t\ , \tag{58}$$

where $C_j(k) = d\omega_j/dk$ is the group velocity on the j^{th} branch of the dispersion curves. For a specified value of t, equation (58) determines one or more values of k_g at any given value of x and the contribution from the integral at that value of x and t is then given approximately by

$$\left[\frac{2\pi i}{t\ \frac{d^2\omega_j}{dk_g^2}}\right]^{\frac{1}{2}} R_j(k_g)\ e^{i(k_g x-\omega_j(k_g)t}\ ,$$

provided $d^2\omega_j/dk_g^2 \neq 0$. At the stationary points of the group velocity, $dC_j/dk = d^2\omega_j/dk^2 = 0$, this result breaks down and the approximation must be carried to higher order, giving the result

$$2\pi\left[\frac{2}{t\ \frac{d^3\omega_j}{dk^3}}\right]^{\frac{1}{3}} R_j(k_g)\ e^{i(k_g x-\omega_j(k_g)t)}\ . \tag{59}$$

Thus the stationary phase approximation at ordinary points of the group velocity curve shows that the long time solution deacays as $t^{-\frac{1}{2}}$ whereas at maxima and minima of the group velocity the decay goes more slowly as $t^{-1/3}$. These are the points corresponding to the wave fronts and it is these wave front solutions, given by equation (59), which dominate at large times. A detailed discussion of these phenomena for a single plate of isotropic elastic material is given in the paper by Jones [9].

4. NUMERICAL METHODS

To carry out the numerical evaluation we choose the values for the material parameters that were previously employed by Green & Baylis [4] and which are derived from measurements carried out by Markham [10] on a carbon fibre/epoxy resin composite. For the inextensible model, these become $c_1^2/c_2^2 = 4.297$ and $c_3^2/c_2^2 = 2.301$. We must also specify the number N, of unit cells forming the laminate and the results reported here relate to the simplest case of N=1 although the computer programmes have been written to cope with the general case of any specified number N of unit cells. In order to obtain the dispersion equation (57) and the expression for the residues given in equation (54), we have made use of the algebraic manipulation programme REDUCE. We provide as basic inputs, the elements p_{ij} of the propagator matrix $\underset{\sim}{P}(h)$ defined in Table 1 and the elements q_{rs} of the matrix $\underset{\sim}{Q}(h)$, obtained by the transformations given in Table 2. The programme then calculates the elements of the matrices $\underset{\sim}{R}$, $\hat{\underset{\sim}{R}}$, $\underset{\sim}{F}$, $\hat{\underset{\sim}{F}}$, using equations (16) for r_{ij} and equivalent equations for f_{ij}, and compounds these to produce the matrices $\underset{\sim}{C}$, $\hat{\underset{\sim}{C}}$ and $\underset{\sim}{D}$. It may be seen from the definition of $\underset{\sim}{D}$ given in equation (22) that det $\underset{\sim}{D} = 1$ so that the eigenvalues λ_1 and λ_2 of $\underset{\sim}{D}$ satisfy the relation $\lambda_1\lambda_2 = 1$. It is also a consequence of the definition that $d_{22} = d_{11}$ and making use of these two results yields explicit expressions for λ_1 and λ_2 as

$$\lambda_1 = d_{11} + \sqrt{d_{11}^2 - 1} = e^{\theta}, \qquad \lambda^2 = d_{11} - \sqrt{d_{11}^2 - 1} = e^{-\theta}, \tag{60}$$

where we define the value of θ by the equation $\cosh \theta = d_{11}$. Using these in the Cayley–Hamilton theorem (equation (23)) we get

$$\underset{\sim}{D}^{n-1} = \frac{\sinh(n-1)\theta}{\sinh \theta}\,\underset{\sim}{D} - \frac{\sinh(n-2)\theta}{\sinh \theta}\,\underset{\sim}{I}, \tag{61}$$

and this expression is employed to replace $\underset{\sim}{D}^{n-1}$ in equations (24) and (30). The REDUCE programme then makes use of equations (27) to evaluate the elements of $\underset{\sim}{S}$ and $\hat{\underset{\sim}{S}}$, finally producing the elements m_{ij} of $\underset{\sim}{M}$ from the definition implicit in equation (30). Having obtained expressions for the elements of $\underset{\sim}{M}$ the REDUCE programme is then applied to obtain an expression for the derivative $dm_{12}/d\hat{s}$ as a function of γ, k, $\hat{s}$ and the material parameters. The outputs from the REDUCE programme consist of a

subroutine to evaluate $m_{12}(k,\hat{s})$ and a subroutine for $R(k,\hat{s}) = m_{22}/(dm_{12}/d\hat{s})$ from which to calculate the residues $R_j(k)$ and these subroutines are incorporated into the computer programme which solves the dispersion equation.

The computer programme to produce the solutions $\omega_j(k)$ to the dispersion equation $m_{12}(k,\hat{s}_j(k) = 0$, where $\hat{s}_j(k) = i\omega_j(k)$, is based on the notion of fixing k, and then, starting from $\omega = 0$, marching up the ω-axis evaluating m_{12} at each step until the required number of zeros of m_{12} have been determined. A zero is indicated by a change of sign of m_{12} at two consecutive values of ω, and by reducing the step length, this zero can be determined to any given degree of accuracy.

Clearly, this method is open to error in that two changes of sign which occur within the same step length will be missed and a change of sign indicates the presence of an odd number of zeros, not necessarily just one. These two possibilities did in fact give rise to problems since adjacent harmonics do, on occasion, run very closely together. In theory, the answer is simple - the step length has to be chosen sufficiently small! However, since a substantial number of harmonics are required, covering a very large set of values of k, the programme would then become excessively expensive in computer time.

A refinement introduced to save running time is to estimate a value of $\omega_j(k)$ and then proceed to a fine search for a zero in its locality. The programme is initialized by using the value for $\omega_j(0)$, derived by solving the dispersion equation at $k = 0$ analytically. It is then possible to use the history of the j^{th} harmonic to estimate the location of the j^{th} root under inspection. For each new value k_{i+1} of k the root corresponding to the fundamental mode, $j = 1$, is the first to be located and this is estimated by $\omega = \omega_1(k_i) - \epsilon$, where $\epsilon = 5\delta k$, and δk is the step length in k. This allows for the possibility of the dispersion curve having a negative gradient. The step length $h_1(k_{i+1})$ in ω is then taken as the minimum of 0.1ϵ and $0.1\{\omega_2(k_i) - \omega_1(k_i)\}$. Thus, if the previous history indicates that the fundamental mode and first harmonic are very close at k_i, the step length at k_{i+1} is chosen as a tenth of the gap at k_i. Otherwise, experience indicates that an increment of $\epsilon/10$ is sufficiently small.

For each of the remaining roots, $\omega_j(k_{i+1})$ for $j > 1$, the first estimate is based not

only on the history of that particular harmonic, but also on the roots already located at k_{i+1} and is given by

$$\omega = \max\{\omega_j(k_i) - \epsilon, \quad \omega_{j-1}(k_{i+1}) + 0.1\ h_{j-1}(k_{i+1})\}.$$

That is, if the root of $\omega_j(k_i)$ is sufficiently far above the previous root at k_{i+1}, $\omega_{j-1}(k_{i+1})$, a substantial amount of computer time can be saved by stepping the first estimate of $\omega_j(k_{i+1})$ over this gap. The step length for locating this root is determined by

$$h_j(k_{i+1}) = \min\left\{\epsilon/10\ ,\ \frac{\omega_{j+1}(k_i)-\omega_j(k_i)}{10}\ ,\ \frac{\omega_j(k_i)-\omega_{j-1}(k_i)}{10}\right\}.$$

This allows for the possibility of the j^{th} harmonic at k_i being very close to either the $(j+1)^{th}$ harmonic or the $(j-1)^{th}$ harmonic.

Once the step length h_j and a first estimate ω for $\omega_j(k_{i+1})$ have been established the procedure for locating the root $\omega_j(k_{i+1})$ is as follows: given k_{i+1} and ω, m_{12} can be evaluated. ω is then increased by the step length h_j and m_{12} recalculated with this new value of ω. We continue to increase ω by the step length until a change of sign of m_{12} is observed. The step length is then reduced by a factor of 10, and the process is repeated using the last value of ω before the change of sign occurred as a new estimate of the root. Once a change of sign has been re-established, the step length is reduced by a further factor of ten and the complete procedure repeated, with termination occurring when $\omega_j(k)$ has been determined to the given degree of accuracy.

Having obtained the solutions of the dispersion equation and the associated residues, we are now in a position to perform the numerical integrations and summation involved in inverting the transforms through expressions of the form (58). To do this, we restrict the range of summation from j = 1 to P and the interval of integration from k = 0 to $\hat{k}$ and rewrite the expression (58) in the approximate form

$$\sum_{j=1}^{\infty} \int_0^{\infty} f_j(k)R_j(k)\ \sin \omega_j(k)t \begin{Bmatrix}\cos kx\\ \sin kx\end{Bmatrix} dk$$

$$\approx \sum_{j=1}^{P} \int_0^{\hat{k}} f_j(k)R_j(k)\ \sin \omega_j(k)t \begin{Bmatrix}\cos kx\\ \sin kx\end{Bmatrix} dk = \int_0^{\hat{k}} H(k,t) \begin{Bmatrix}\cos kx\\ \sin kx\end{Bmatrix} dk\ , \quad (62)$$

where

$$H(k,t) = \sum_{j=1}^{P} f_j(k) R_j(k) \sin \omega_j(k) t . \tag{63}$$

Of the two approximations involved in equation (62), the effect of restricting the summation to a finite number of roots (P) cannot be evaluated without some estimate of the contributions arising from the residues of the excluded branches and in general such an estimate is not available. The effect of restricting the integral to a finite range is, however, immediately calculable. To do this it is convenient to define the function G(k,t) such that

$$\int_0^{\infty} H(k,t) \begin{Bmatrix} \cos kx \\ \sin kx \end{Bmatrix} dk = \tfrac{1}{2} \int_{-\infty}^{\infty} G(k,t)\, e^{ikx}\, dk , \tag{64}$$

so that if the integrand is H(k,t)cos kx, then G(k,t) = H(k,t) for $k > 0$ and G(k,t) = H(-k,t) for $k < 0$, whereas if the integrand is H(k,t)sin kx then G(k,t) = H(k,t) for $k > 0$ and G(k,t) = -H(-k,t) for $k < 0$. Letting F(x,t) denote the function whose Fourier transform is G(k,t), we have that

$$G(k,t) = \int_{-\infty}^{\infty} F(y,t)\, e^{iky}\, dy \tag{65}$$

and using this gives

$$\begin{aligned} \int_0^{\hat{k}} H(k,t) \begin{Bmatrix} \cos kx \\ \sin kx \end{Bmatrix} dk &= \tfrac{1}{2} \int_{-\hat{k}}^{\hat{k}} G(k,t)\, e^{ikx}\, dx, \\ &= \tfrac{1}{2} \int_{-\infty}^{\infty} F(y,t) \int_{-\hat{k}}^{\hat{k}} e^{ik(x-y)}\, dk\, dy, \\ &= \int_{-\infty}^{\infty} F(y,t)\, \frac{\sin \hat{k}(x-y)}{(x-y)}\, dy, \\ &= \hat{F}(x,t). \end{aligned} \tag{66}$$

The function $\hat{F}(x,t)$ defined in equation (66) is the convolution of the true signal F(x,t) with the function $(\sin \hat{k}x)/x$ and exhibits the phenomenon of "windowing". This phenomenon produces a spurious oscillation of wavelength $2\pi/\hat{k}$ and in order to reduce the effect of the oscillation we have made use of the Hamming window function s(k) defined by

$$s(k) = \alpha + (1-\alpha)\cos\left[\frac{k\pi}{\hat{k}}\right] , \tag{67}$$

where α is some parameter satisfying $0 < \alpha < 1$. The procedure is to replace the integrand over the finite range $(0,\hat{k})$ by the product of the integrand with s(k) to give a new approximation $\hat{F}_H(x,t)$ given by

$$\begin{aligned}\hat{F}_H(x,t) &= \int_0^{\hat{k}} s(k)H(k,t) \begin{Bmatrix}\cos kx\\ \sin kx\end{Bmatrix} dk ,\\ &= \tfrac{1}{2}\int_{-\hat{k}}^{\hat{k}} s(k)G(k,t)dk ,\\ &= \alpha\,\hat{F}(x,t) + \frac{(1-\alpha)}{2}\left\{\hat{F}(x-\tfrac{\pi}{\hat{k}},t) + \hat{F}(x+\tfrac{\pi}{\hat{k}},t)\right\} .\end{aligned} \tag{68}$$

The convolution terms in the braces are each half a wavelength out of phase with the convolution $\hat{F}(x,t)$ and this serves to dampen out the oscillation. In evaluating our numerical results we have used the value $\alpha = 0.54$ recommended by Hamming [8]. Note that both $\hat{F}(x,t)$ and $\hat{F}_H(x,t)$ tend to the true signal as $\hat{k} \to \infty$. There is one further approximation required in order to perform the integration and this consists of replacing the integral by a finite sum of terms. This has been done using the trapezium rule, with interval length $\hat{k}/M$ and it can be shown that this procedure is equivalent to replacing the convolution integral $\hat{F}(x,t)$ defined by equation (66) by the convolution $\tilde{F}(x,t)$ defined by

$$\tilde{F}(x,t) = \frac{\hat{k}}{2M}\int_{-\infty}^{\infty} F(y,t)\,\frac{\sin\hat{k}(x-y)\cos\frac{\hat{k}}{2M}(x-y)}{\sin\frac{\hat{k}}{2M}(x-y)}\,dy . \tag{69}$$

The calculated result is then the Hamming function of this convolution and is given by

$$\tilde{F}_H(x,t) = \alpha\tilde{F}(x,t) + \frac{(1-\alpha)}{2}\left\{\tilde{F}(x-\tfrac{\pi}{\hat{k}},t) + \tilde{F}(x+\tfrac{\pi}{\hat{k}},t)\right\} . \tag{70}$$

The convolution $\tilde{F}(x,t)$ tends to $\hat{F}(x,t)$ in the limit as M increases to infinity, but for finite values of M the function defined by equation (69) is periodic in x with wavelength $4\pi M/\hat{k}$ and the numerical integration procedure is therefore limited to values of x satisfying $0 \leq x < 4\pi M/\hat{k}$.

In performing the numerical integration we have chosen as unit of length the half thickness h of each ply and as unit of time the quantity h/c_1. For a given value of γ, the dispersion equation has been solved for eighteen modes (P=18) with values of kh ranging from zero to 20 ($\hat{k}$=20/h) in steps of 0.002, corresponding to M = 10,000. This gives rise to 180,000 values of $\omega_j(k)$ and an equal number of values of the residues $R_j(k)$ which form the data matrix for the numerical inversions. The procedure for this is to specify a value of t and to form the sums H(k,t) appropriate to the particular displacement or stress being evaluated. Each sum H(k,t) is multiplied by the corresponding value of the Hamming factor s(k) and the product is stored. Using the trapezium rule, the integral is then evaluted for a range of values of x from x = 0 to $x = c_1 t$ in steps of $\Delta x = 2\pi/\hat{k}$.

5. RESULTS

The results we present in this section are in the form of graphs and fall into three sets. The first set consists of the dispersion curves, relating the scaled frequency $\omega h/c_2$ to the non-dimensional wave number kh for a range of values of the angle of propagation γ satisfying $0^0 \leq \gamma \leq 90^0$. Propagation at angles outside this range may be obtained from these by symmetry. The dispersion curves together with their associated residues provide the fundamental information required to invert the transforms, but we have seen in Section 3 that the long time solution is governed by the group velocity curves and in particular that the wave fronts are related to the maxima and minima of the group velocity. Our second set of results displays a selection of group velocity curves at different values of the angle of propagation γ. Finally we present a set of curves showing the variation of displacements and stresses at the outer surfaces of the plate as functions of the propagation distance x at various times. These results are derived by numerical integration along the dispersion curves and are presented here for propagation at the angle $\gamma = 60^0$ only. Calculation of each of these latter sets of results involves the use of 360,000 stored values for each angle of propagation γ and results for other angles of propagation will appear elsewhere.

The laminate with which we are dealing consists of an arrangement of 4 plies which is symmetric about the middle surface. It may be shown that, in consequence, the dispersion equation factorizes into two distinct equations, one associated with the symmetric (longitudinal) motion of the plate and the other with the antisymmetric (flexural) motion. The dispersion curves for the fundamental modes of these two equations have been examined in detail by Baylis [11] and Baylis and Green [4],[5]. They show that the limiting velocity of short waves (large kh) propagating at angle γ is either the velocity of Rayleigh type surface waves at angle γ in the outer material or of shear waves at angle γ in the inner material according as to whether γ is less than or greater than some critical value γ_c, which, for the parameters employed here, is 46.3^0. The limiting short wavelength velocity of all the other harmonics is either the velocity of shear waves at angle γ in the outer material or the velocity of shear waves at an angle γ in the inner material, according as to whether γ is less than or greater than 45^0.

These are the speeds $v_{1s} = (c_5^2c^2+c_2^2s^2)^{\frac{1}{2}}$ in the inner material (material *1*) and $v_{2s} = (c_5^2s^2+c_2^2c^2)^{\frac{1}{2}}$ in the outer material (material *2*) at which $p_2 = 0$ and $q_2 = 0$ respectively. We can also associate with each material a dilatational wave speed $v_{1d} = (c_4^2s^2+c_3^2c^2)^{\frac{1}{2}}$ and $v_{2d} = (c_4^2c^2+c_3^2s^2)^{\frac{1}{2}}$ at which $p_1 = 0$ and $q_1 = 0$, respectively. For values of $\gamma < 45^0$ we have that $v_{1d} < v_{2d}$ but $v_{1s} > v_{2s}$ with the inequalities reversed for $\gamma > 45^0$. (Note that $v_{1d} \geq v_{1s}$ and $v_{2d} \geq v_{2s}$ for all γ.) On any branch of a dispersion curve at points where the phase velocity $v = \omega/k$ is greater than the supremum (v_{1d},v_{2d}) all of p_1, p_2, q_1, q_2 are pure imaginary and the solutions correspond to progressive waves in all regions. As the phase velocity drops below the supremum (v_{1d}, v_{2d}) either p_1 or q_1 becomes real and the associated dilatational wave motion is evanescent. Continued reduction in v makes both p_1 and q_1 real, corresponding to evanescent dilatational disturbances in both materials and as v decreases further with increasing k the supremum (v_{1s}, v_{2s}) is reached making either p_2 or q_2 real and the motion subequently involves a progressing shear wave in one material with all the other waves being evanescent.

Figure 1 shows a total of 26 branches (13 each of the symmetric and antisymmetric modes) of the dispersion curves for propagation at the angle $\gamma = 90^0$. All modes except the fundamental mode of the antisymmetric motion exhibit a cut-off frequency in the long wavelength limit $kh \to 0$. A striking feature of the graph is the existence of the two clear ghost lines brought about by the osculation of the branches. (These are particularly clear when the graph is viewed at almost grazing incidence). These ghost lines have slopes $\omega/k = c_1$ and $\omega/k = c_3$, which correspond to $v = v_{1d}$ and $v = v_{2d} = v_{2s}$ respectively at $\gamma = 90^0$. As the dispersion curves approach the first ghost line from the left they exhibit the plateau and step phenomenon described by Redwood [12]. Along the plateaux the curves are almost parallel to the ghost line, with the phase velocity and group velocity virtually constant at the value given by the slope of the ghost line. On the steps the phase velocity exhibits a small but sudden drop, with an associated drop in the group velocity, either ending up on the next plateau, if still to the left of the ghost line, or passing through and moving rapidly towards the second ghost line, where the phenomenon is repeated. On crossing the second ghost line

the dispersion curves are virtually parallel, with the slope $\omega/k = c_2$, as they tend to the limiting velocity v_{1s} of shear waves in the inner material as $kh \to \infty$. Figures 2, 3, 4, 5, each contain two sets of dispersion curves, set (a) corresponding to symmetric modes and set (b) to antisymmetric modes at angles 60^0, 45^0, 30^0 and 0^0 respectively. As in Figure 1, all the branches except the fundamental antisymmetric mode (curves (b), exhibit a cut-off frequency in the long wavelength limit $kh \to 0$. The curves again display the ghost lines through not to such a marked extent as in Figure 1 since the number of curves is now either 9 or 10 in each figure. Despite this, it is still possible to identify three ghost lines in Figures 2 and 4 as opposed to two in Figures 1, 3 and 5 for each of which two of the 4 speeds v_{1d}, v_{2d}, v_{1s}, v_{2s} become equal.

Figures 6, 7 and 8 show graphs of the group velocity C_g, against kh. These have been obtained by numerical differentiation of the dispersion curves, using a central difference formula. Figure 6 corresponds to the first 20 of the 26 dispersion curves, at $\gamma = 90^0$, shown in Figure 1. On the scale of the figure, the two ghost velocities are $v_{1d} = c_1 = 3.25$ and $v_{2d} = v_{2s} = c_3 = 2.38$ with the limiting velocity at $v_{1s} = c_2 = 1.57$. The curves clearly show the plateau and step regions associated with both ghost velocities, displaying local maxima which approach c_1, followed by local maxima close to c_3 and tending to c_2 as kh increases. Figure 7a shows the first five harmonics of the symmetric modes at $\gamma = 60^0$ and Figure 7b gives the first five harmonics of the antisymmetric mode for the same angle. At this angle of propagation we have $v_{1d} = 3.06$, $v_{2d} = 2.62$, $v_{2s} = 2.20$ and $v_{1s} = 1.81$. None of our curves approaches the value of v_{1d} which is not surprising since it may be seen from Figure 2 that the first ghost line is associated with harmonics of order greater than five. It may be seen that there is one of the five curves of Figure 7a which has a maximum at $C_g = 2.4$, this being the highest of the five harmonics which may be seen from 2a to have a plateau close to the second ghost line. Both Figures 7a and 7b possess harmonics with maxima close to $C_g = 2.20$, corresponding to the third ghost line associated with this angle of propagation. The curves shown in Figure 8 relate to the angle $\gamma = 0$, the set (a) being the first 5 symmetric modes and the set (b) the first 5 antisymmetric modes. Here, as for $\gamma = 90^0$, there are only two ghost lines at

$v_{2d} = c_1 = 3.25$ and $v_{1d} = v_{1s} = c_3 = 2.38$, with the lowest shear velocity being $v_{2s} = c_2 = 1.57$, in the outer material. None of the curves in 8(a) and 8(b) have maxima approaching the first ghost velocity but the maxima at the second are very clearly exhibited in both sets. We have remarked in Section 3 that the local maxima and minima of the group velocity curves correspond to the wavefronts, which are expected to dominate the disturbance at large times. The higher harmonics shown in Figures 6–8 exhibit long flat maxima at the ghost velocities, which do not appear in the fundamental modes. It is pointed out by Jones [9] for an isotropic plate, that the residues associated with the higher harmonics are small compared with those arising from the lowest modes and our numerical results show this to be the case here also. Nevertheless, the total contribution arising from the succession of plateau regions associated with these high harmonics at the ghost velocities, will give rise to precursor waves which are not exhibited by the solution from the fundamental mode alone nor from approximate plate theories designed to reproduce the fundamental mode.

The remaining figures (9–16) display the variation of displacements and stresses as functions of distance from the impact point at different values of the reduced time $T = c_1 t/h$ for propagation at an angle $\gamma = 60^0$. Figures 9a and 9b show the normal displacement u_1 at the upper and lower surfaces respectively. Each shows the variation with distance at times T = 10, 20, 30, 40, 50. Figures 10a and 10b show the upper and lower normal surface displacements at considerably larger times, namely T = 100, 200 and 500. Figures 11–14, inclusive, display the normal displacement u_1, tangential displacement u_2, the discontinuous shear traction t_{13} along the fibre direction and the in-plane shear stress component t_{23} respectively, all at time T = 40. Each figure presents results at both the upper and lower surfaces, derived from using the transforms given in equation (43) at the upper surface and their equivalents at the lower surface. It may be seen from equations (43) that the in-plane stress components t_{22} and t_{33} have terms in the transforms which involve $kV_1^{(n)}$ and these terms may be evaluated directly from the stress term t_{23} by an appropriate scaling. The normal displacements, shown in Figure 11 are obtained by inverting the transform given by equation (33) using the Hamming window. The results show little trace of a spurious oscillation and the

windowing appears to be successful. The discontinuous tangential stress t_{13} shown in Figure 13 is in effect derived from this displacement by differentiation with respect to x. This serves to roughen the numerical results and there is now some indication of a superimposed oscillation. The tangential displacement u_2 is obtained by inverting the first expression in equation (43) which involves multiplying the normal displacement transform by the factor p_{43}/p_{44}. The results shown in Figure 12 exhibit a considerable windowing effect, despite the use of the Hamming technique and this is further accentuated in Figure 14 since the in-plane tangential stress is essentially the x derivative of the tangential displacement.

In order to examine the effects of the harmonics, we have calculated the normal and tangential components of displacements associated with the fundamental mode of the symmetric and antisymmetric waves at T = 40. These are shown in Figure 15 and it may be seen that each gives a disturbance commencing at $x \approx 27$, corresponding to a speed v = 2.19 in the units we are employing. These curves may be compared with those shown in Figure 11 wich are calculated using a total of 18 modes (9 each of the symmetric and antisymmetric) and which show a disturbance commencing at $x \approx 32$ corresponding to v = 2.60. Finally, in Figure 16 we show the normal and tangential upper surface displacements at $T = 40^0$ calculated using 10 modes only (5 each of the symmetric and antisymmetric). We note that these produce a disturbance at only slightly larger values of x than the two fundamental modes. This is consistent with the fact that the highest ghost speed is only displayed by the harmonics of order higher than five in each mode of wave motion. We further note that these curves show little evidence of oscillation in the tangential displacement as compared with that displayed in Figure 12. This is consistent with the fact that all ten first harmonics have crossed the lowest ghost line before the cut off wave number $\hat{k}$ is reached. The motion associated with each of these harmonics is then a propagating shear disturbance largely confined to the inner core and these harmonics make no contribution to the surface displacements at values close to $\hat{k}$ so that there is no effect to be expected from curtailing the integrals.

ACKNOWLEDGEMENTS

We take this opportunity to express our gratitude to Lt. Col. J.G.R. Hansen, U.S.A.F., E.O.A.R.D., for his support of this work through the award of grant AFOSR-86-0330. We also express our heartfelt thanks to Mrs. Anne Perkins for her patience and consideration in the typing of this work.

REFERENCES

[1] G. C. Everstine and A. C. Pipkin, 1971,
Z. Angew. Math. Phys. **22**, 825–834. Stress channelling in transversely isotropic elastic composites.

[2] W. A. Green, 1982, Quart. J. Mech. Appl. Math. **35**, 485–507.
Bending waves in strongly anisotropic elastic plates.

[3] W. A. Green and D. Milosavljević, 1985, Int. J. Solids & Structures, **21**, 343–353.
Extensional waves in strongly anisotropic elastic plates.

[4] E. R. Baylis and W. A. Green, 1986, J. Sound & Vibr. **110**, 1–26.
Flexural waves in fibre–reinforced laminated plates.

[5] E. R. Baylis and W. A. Green, 1986, J. Sound & Vibr. **111**, 181–190.
Flexural waves in fibre–reinforced laminated plates, part II.

[6] F. Gilbert and G. E. Backus, 1966, Geophysics, **31**, 326–332.
Propagator matrices in elastic waves and vibration problems.

[7] W. A. Green and E. R. Baylis, 1986, Archives of Mechanics, **31**, 301–317.
Wave propagation in laminated plates of inextensible transversely isotropic elastic material.

[8] R. W. Hamming, 1977, Digital Filters, Prentice–Hall, London.

[9] R. P. N. Jones, 1964, Quart. J. Mech. Appl. Math. **17**, 401–421.
Transverse impact waves in a bar under conditions of plane–strain elasticity.

[10] M. F. Markham, 1970, Composites **1**, 145–149.
Measurement of the elastic constants of fibre composites by ultrasonics.

[11] E. R. Baylis, 1987, Ph.D. Thesis, University of Nottingham.
Wave propagation in fibre–reinforced laminates.

[12] M. Redwood, 1960, Mechanical waveguides, New York, Pergamon Press.

$$\underline{P}(h) = \begin{pmatrix} \alpha C_1+(1-\alpha)C_2 & \frac{\alpha s S_1}{p_1}+(1-\alpha)\frac{p_1 S_2}{s} & -\frac{2\alpha^2 s^3 S_1}{(1-\alpha)p_1}+(1-\alpha)2p_2 S_2 & 2\alpha s(C_1-C_2) \\ (1-\alpha)\frac{p_1 S_1}{s}+\frac{\alpha s S_1}{p_2} & (1-\alpha)C_1+\alpha C_2 & -2\alpha s(C_1-C_2) & 2(1-\alpha)p_1 S_1-\frac{2\alpha^2 s^2 S_2}{(1-\alpha)p_2} \\ -\frac{(1-\alpha)}{2}\left(\frac{p_1 S_1}{s^2}-\frac{S_1}{p_2}\right) & -\frac{(1-\alpha)}{2s}(C_1-C_2) & \alpha C_1+(1-\alpha)C_2 & -(1-\alpha)\frac{p_1 S_1}{s}-\frac{\alpha s S_2}{p_2} \\ \frac{(1-\alpha)}{2s}(C_1-C_2) & \frac{(1-\alpha)}{2}\left(\frac{S_1}{p_1}-\frac{p_2 S_2}{s^2}\right) & -\frac{\alpha s S_1}{p_1}-(1-\alpha)\frac{p_2 S_2}{s} & (1-\alpha)C_1+\alpha C_2 \end{pmatrix}$$

TABLE 1 Elements of the propagator matrix P(h).

The terms appearing in the matrix are defined by $s = \sin\gamma$, $c = \cos\gamma$

$S_1 = \sinh p_1 kh$, $C_1 = \cosh p_1 kh$, $S_2 = \sinh p_2 kh$, $C_2 = \cosh p_2 kh$.

$$p_1^2 \quad \frac{(c_1^2 s^2+c_3^2 c^2-v^2)}{c_1^2}, \qquad p_2^2 = \frac{(c_2^2 s^2+c_3^2 c^2-v^2)}{c_2^2}, \qquad v^2 = -\frac{\hat{s}^2}{k^2}, \qquad \alpha = 1-\frac{2c_2^2 s^2}{(v^2-c_3^2 c^2)}$$

$p_1 \to q_1$, $p_2 \to q_2$, $\alpha \to \hat{\alpha}$, $s \to c$,

$S_1 \to \hat{S}_1$, $C_1 \to \hat{C}_1$, $S_2 \to \hat{S}_2$, $C_2 \to \hat{C}_2$,

TABLE 2 Transformation taking elements p_{ij} into q_{ij}.

The terms appearing in the table are defined by

$$q_1^2 = \frac{(c_1^2 c^2+c_3^2 s^2-v^2)}{c_1^2}, \qquad q_2^2 = \frac{(c_2^2 c^2+c_3^2 s^2-v^2)}{c_2^2},$$

$$\hat{\alpha} = 1-\frac{2c_2^2 c^2}{(v^2-c_3^2 s^2)}, \qquad \hat{S}_1 = \sinh q_1 kh, \qquad \hat{C}_1 = \cosh q_1 kh,$$

$\hat{S}_2 = \sinh q_2 kh$, $\hat{C}_2 = \cosh q_2 kh$.

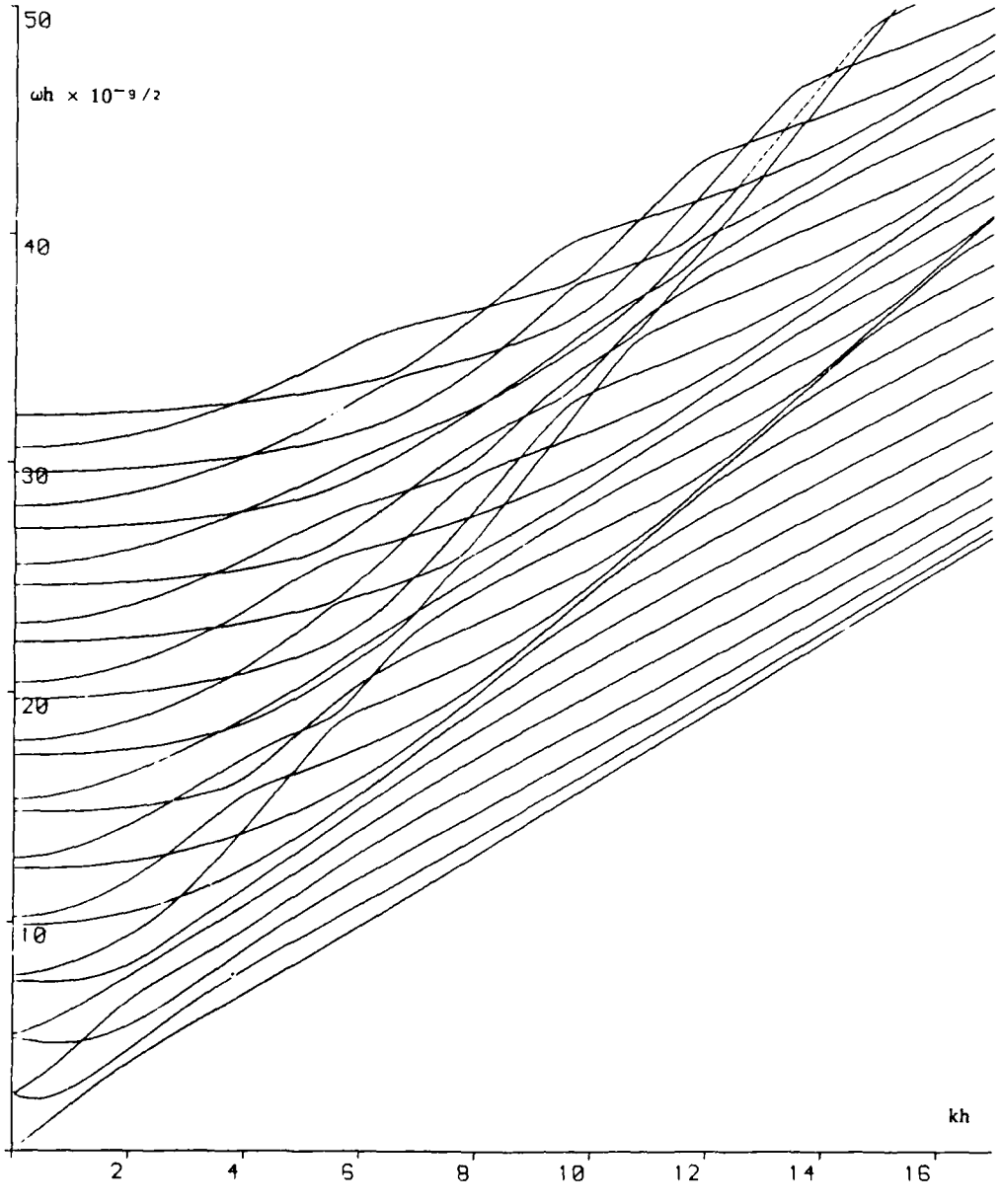

Figure 1. Dispersion curves for propagation at $\gamma = 90^{\circ}$.

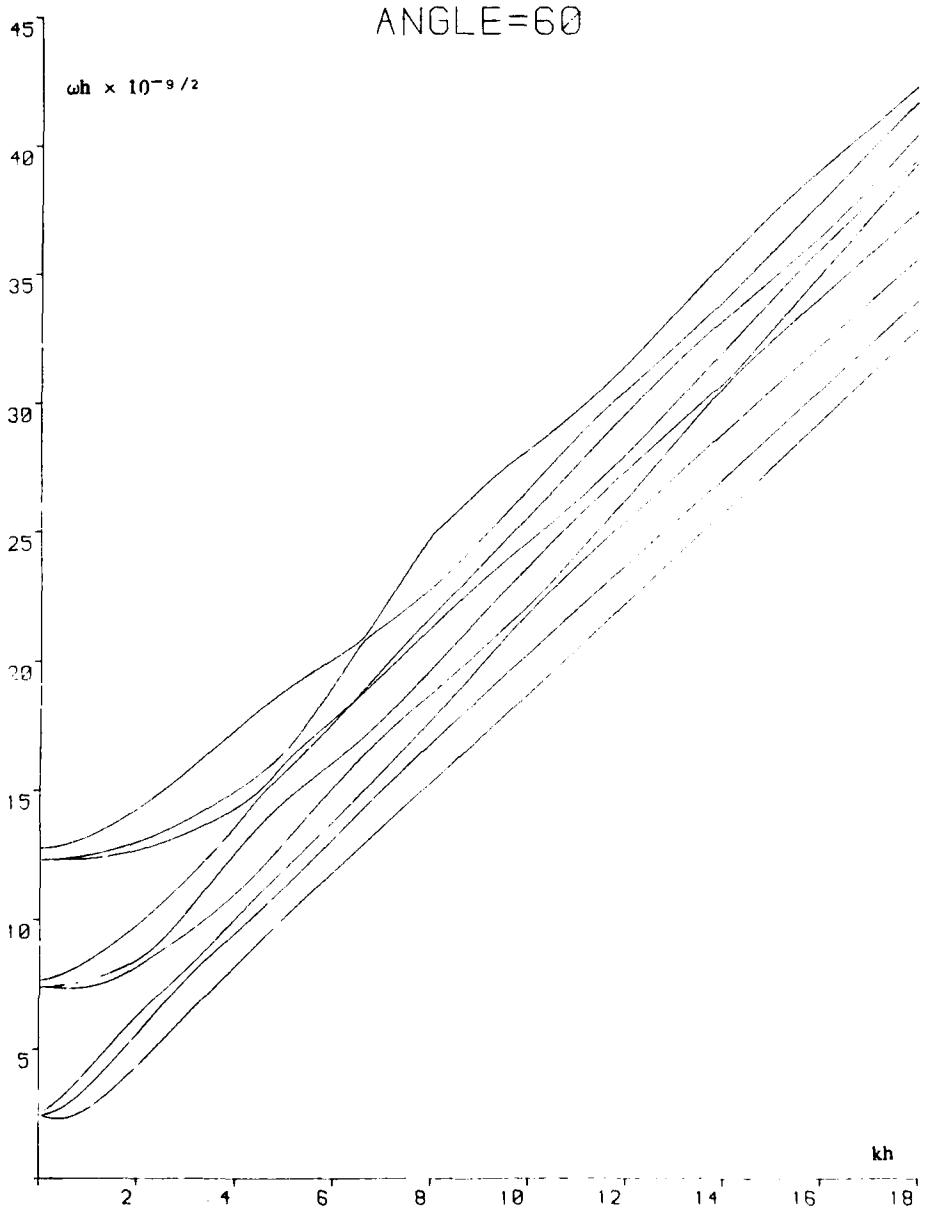

Figure 2a. Dispersion curves for symmetric modes of propagation at $\gamma = 60^0$

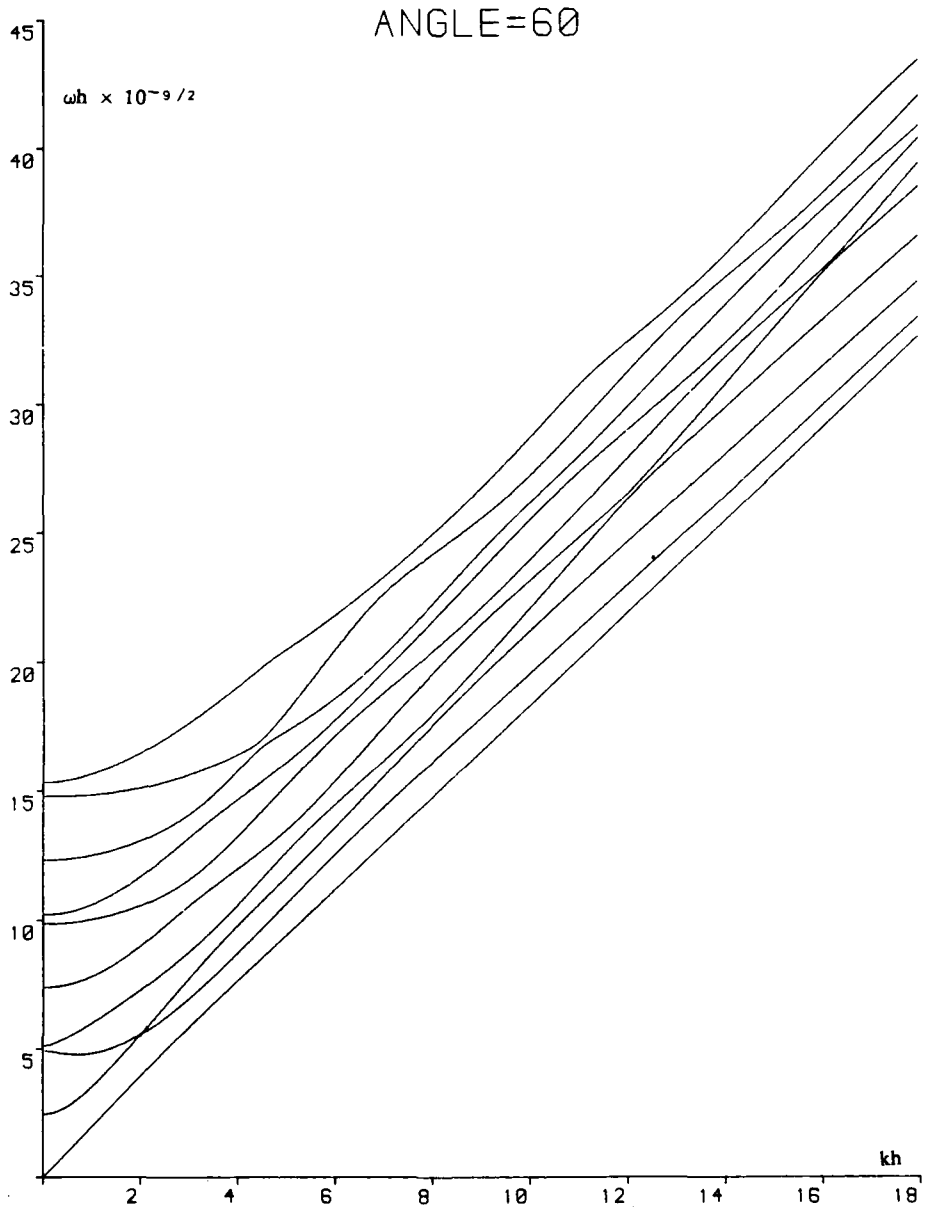

Figure 2b. Dispersion curves for antisymmetric modes of propagation at $\gamma = 60^{0}$

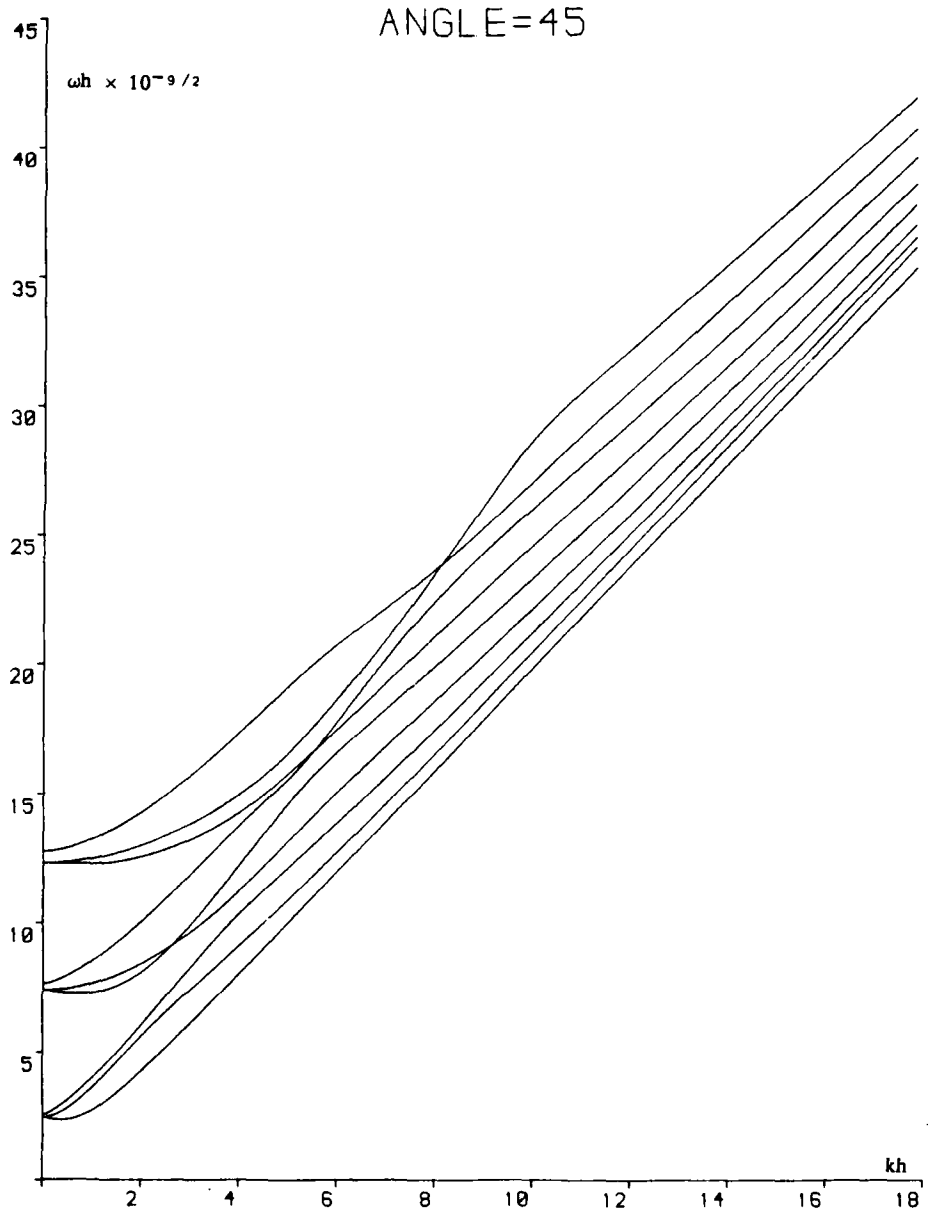

Figure 3a. Dispersion curves for symmetric modes of propagation at $\gamma = 45^0$

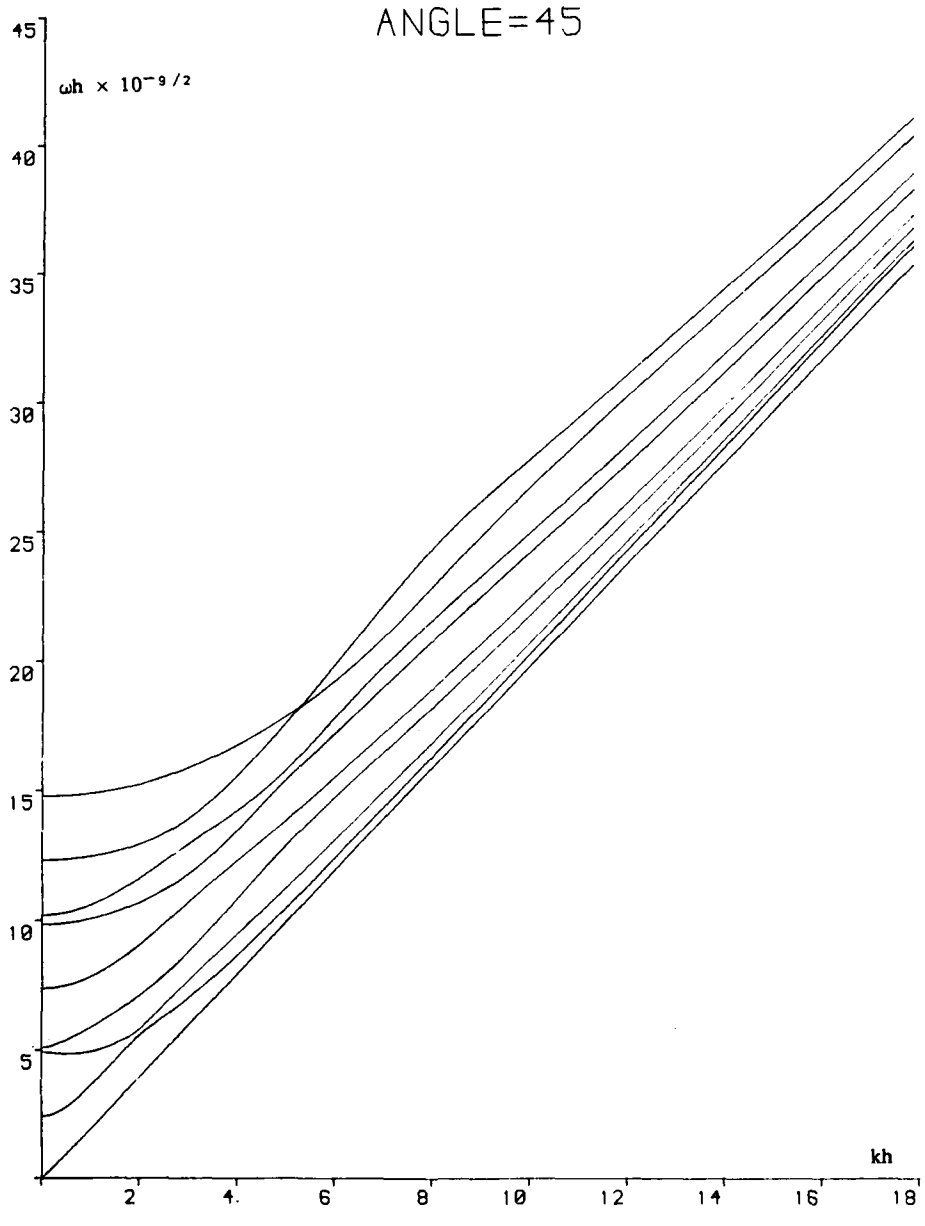

Figure 3b. Dispersion curves for antisymmetric modes of propagation at $\gamma = 45^0$

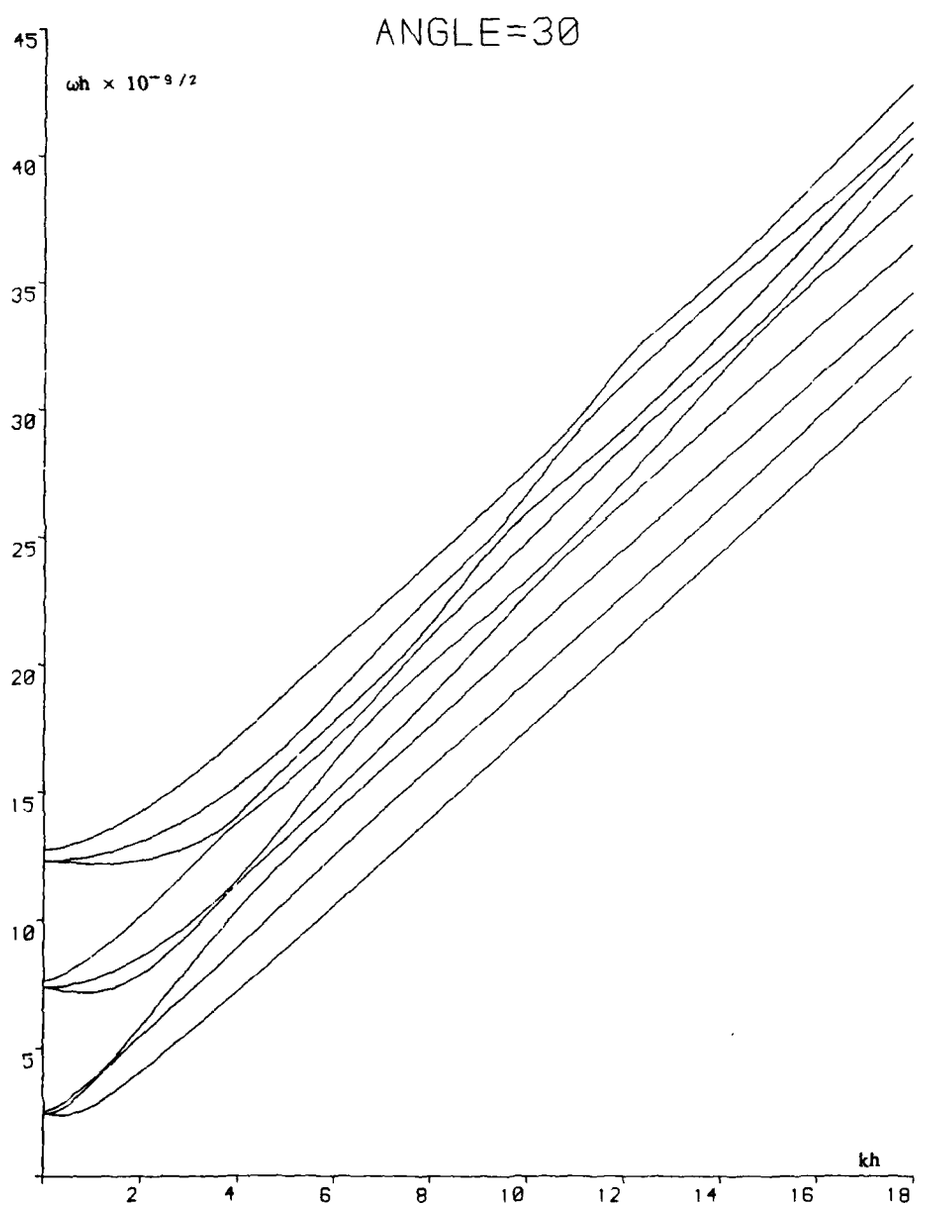

Figure 4a. Dispersion curves for symmetric modes of propagation at $\gamma = 30^0$

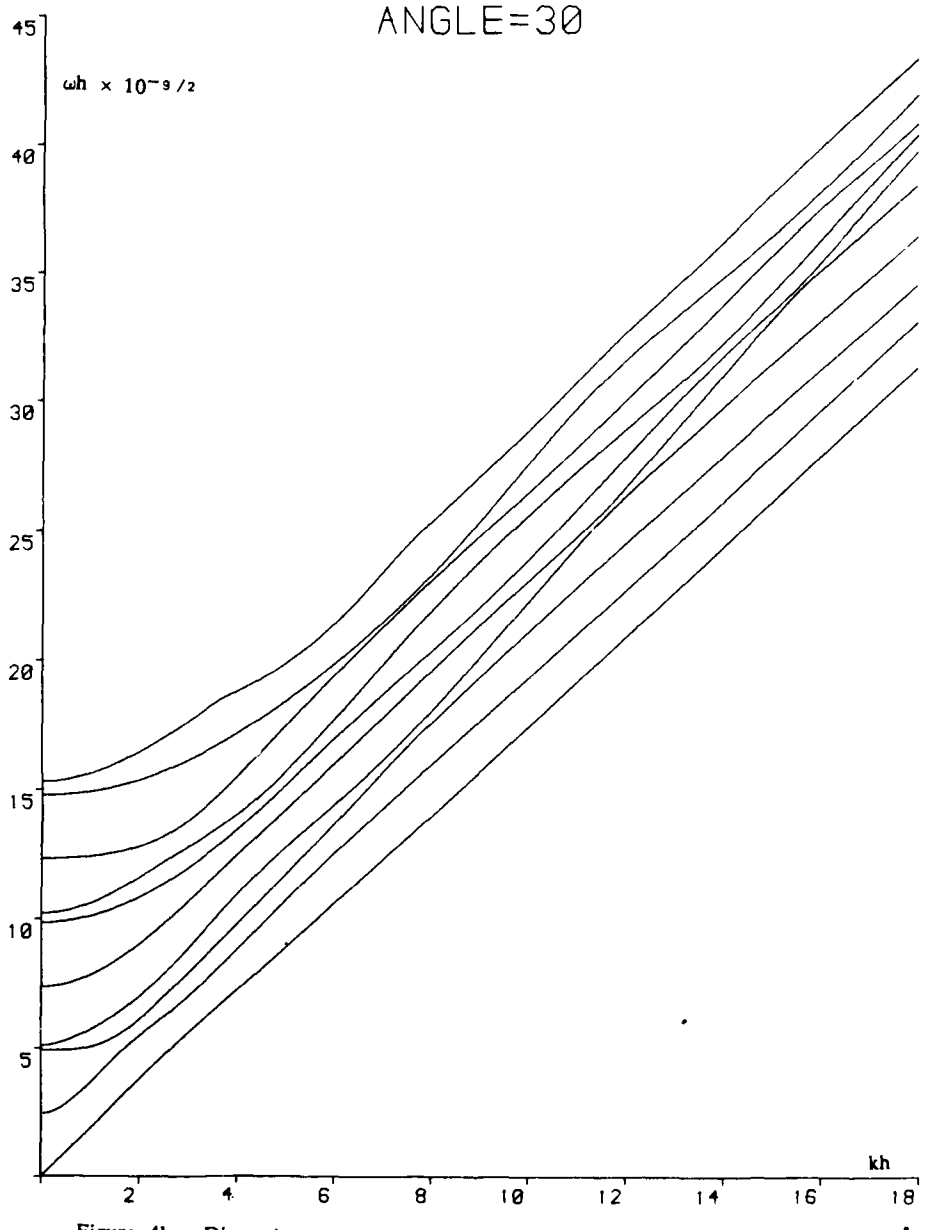

Figure 4b. Dispersion curves for antisymmetric modes of propagation at $\gamma = 30^0$

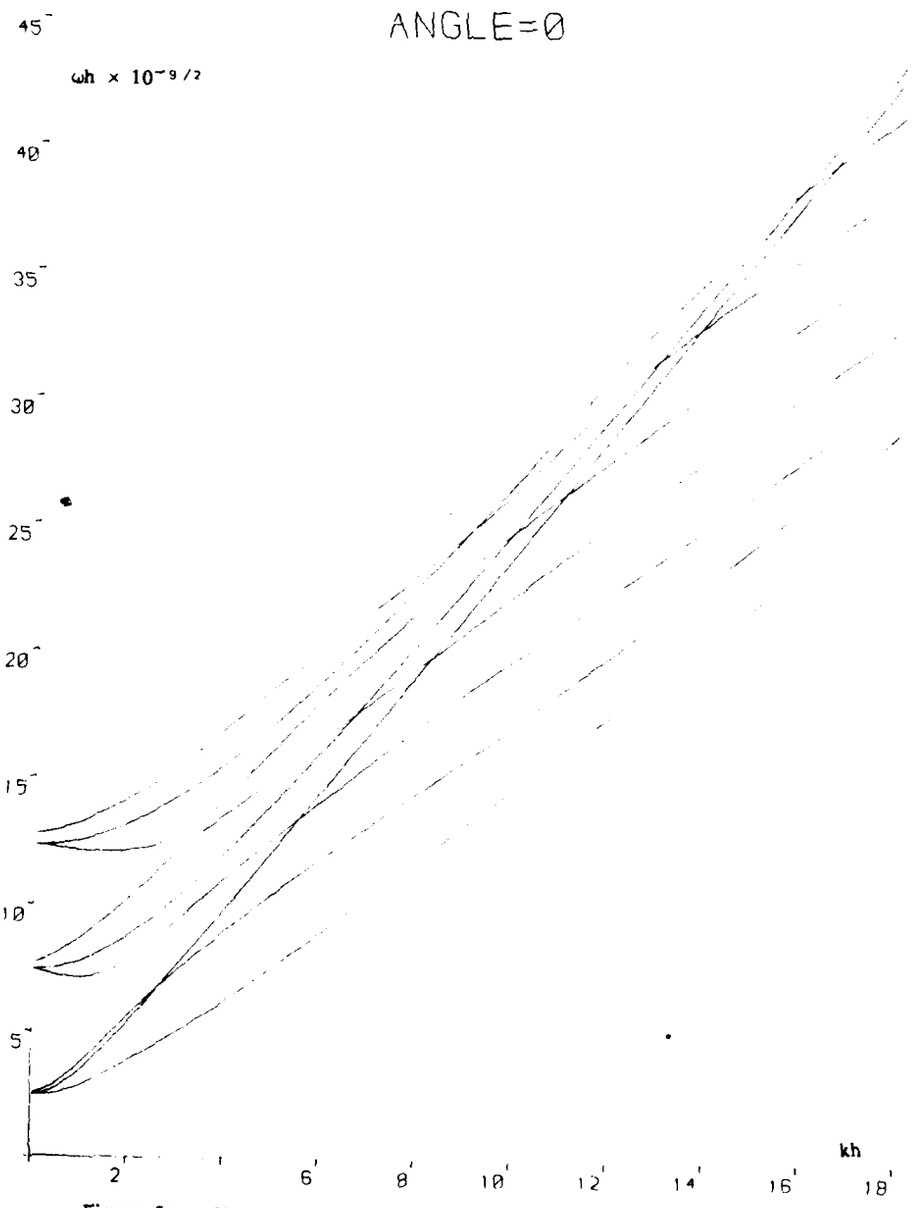

Figure 5a. Dispersion curves for symmetric modes of propagation at $\gamma = 0^0$

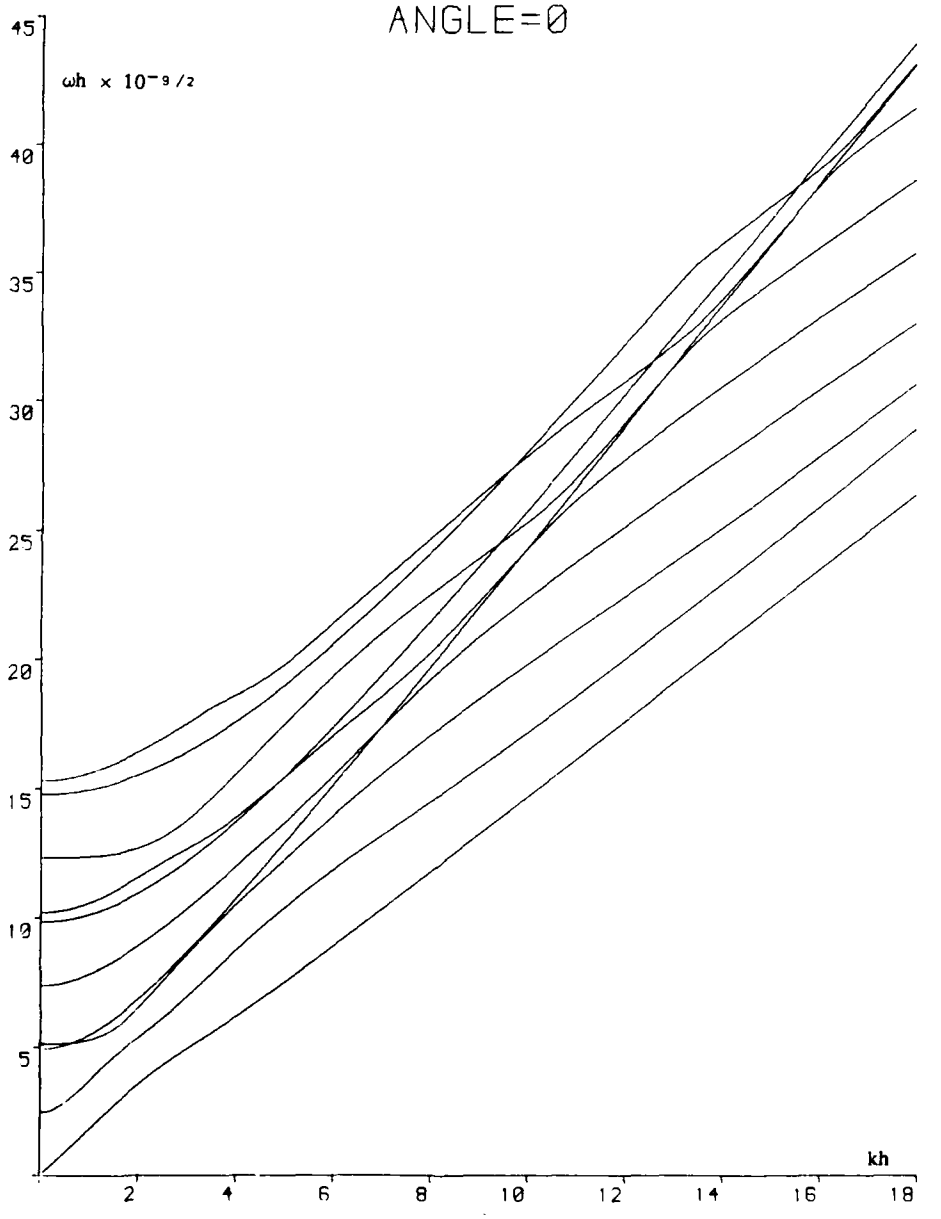

Figure 5b. Dispersion curves for antisymmetric modes of propagation at $\gamma = 0^0$

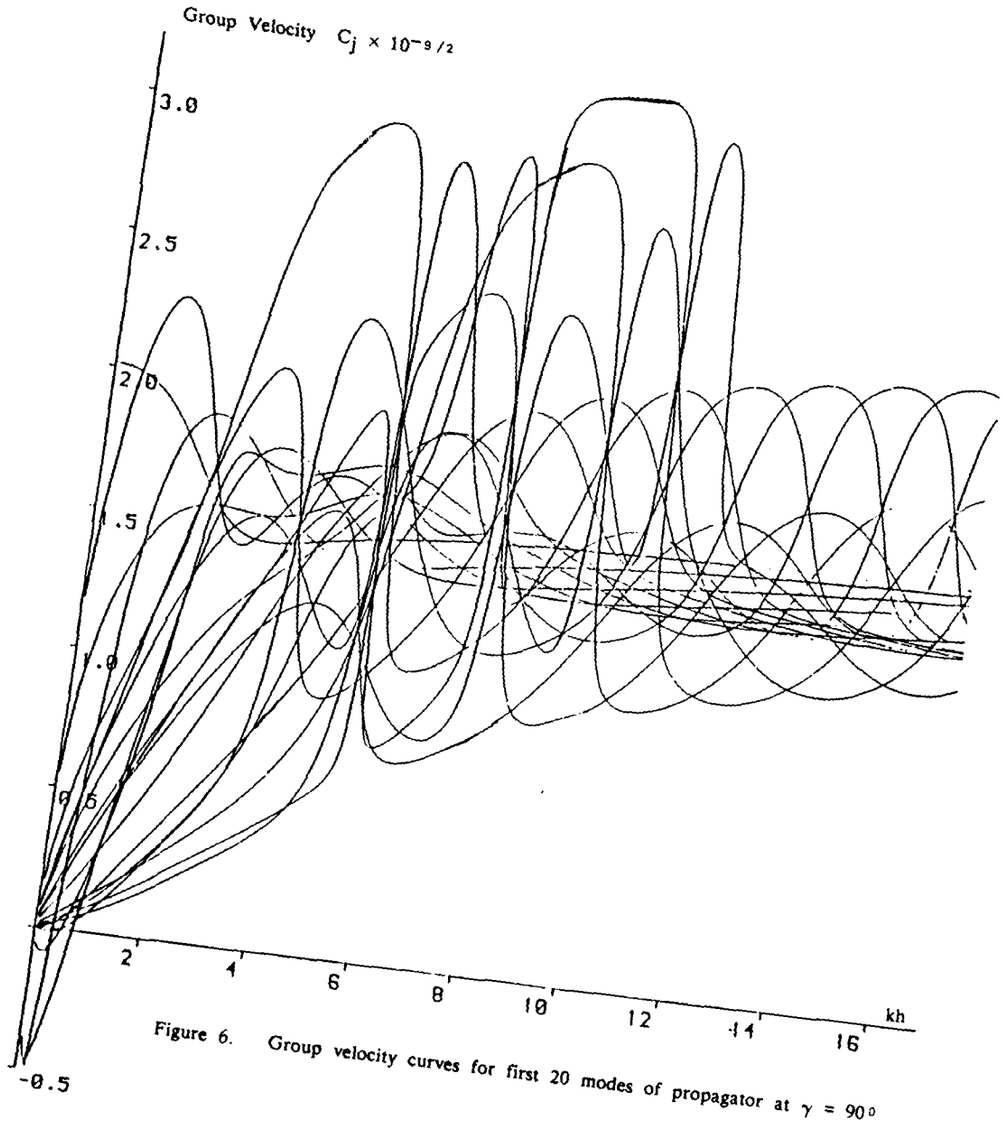

Figure 6. Group velocity curves for first 20 modes of propagator at $\gamma = 90^0$

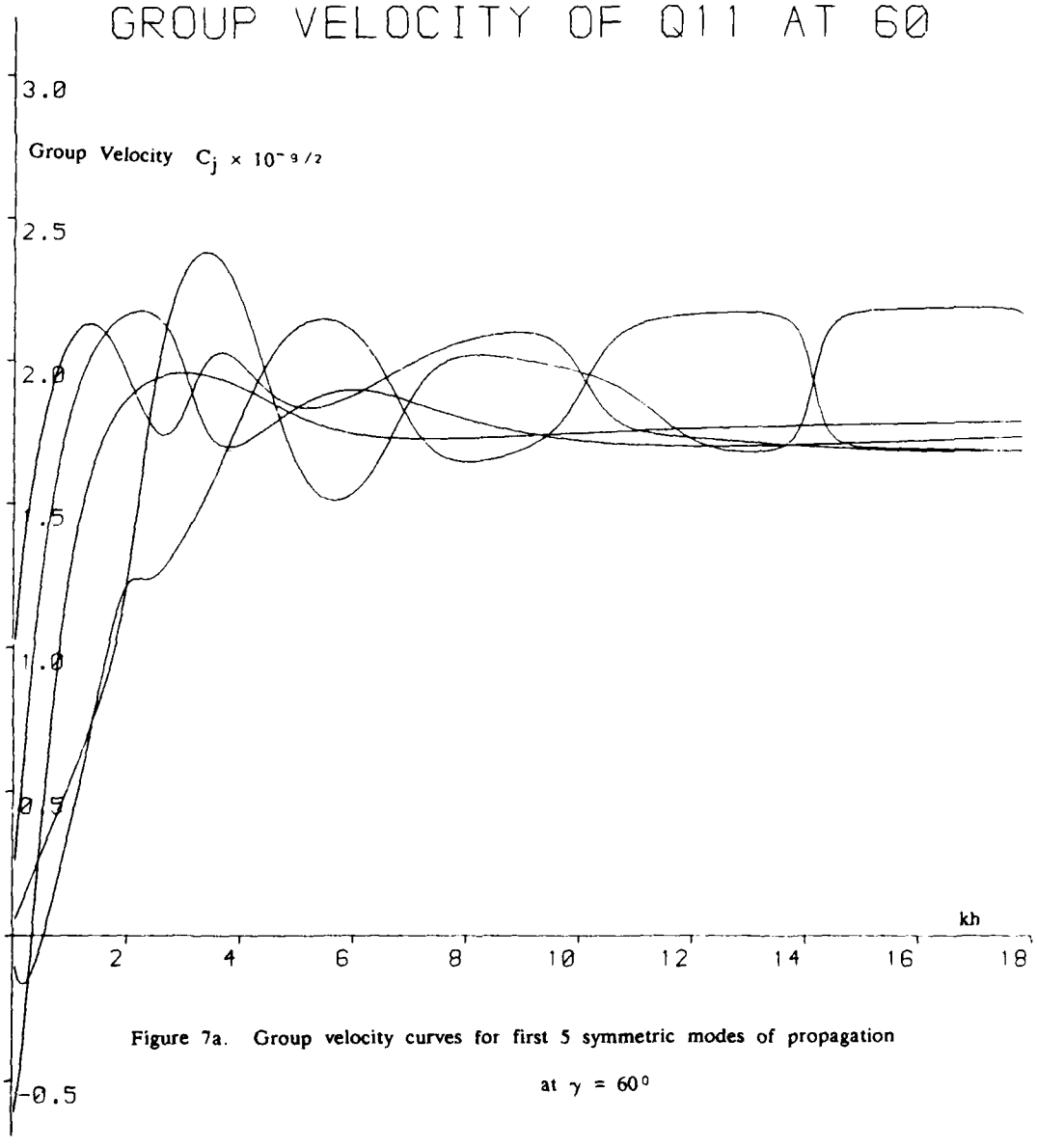

Figure 7a. Group velocity curves for first 5 symmetric modes of propagation at $\gamma = 60^0$

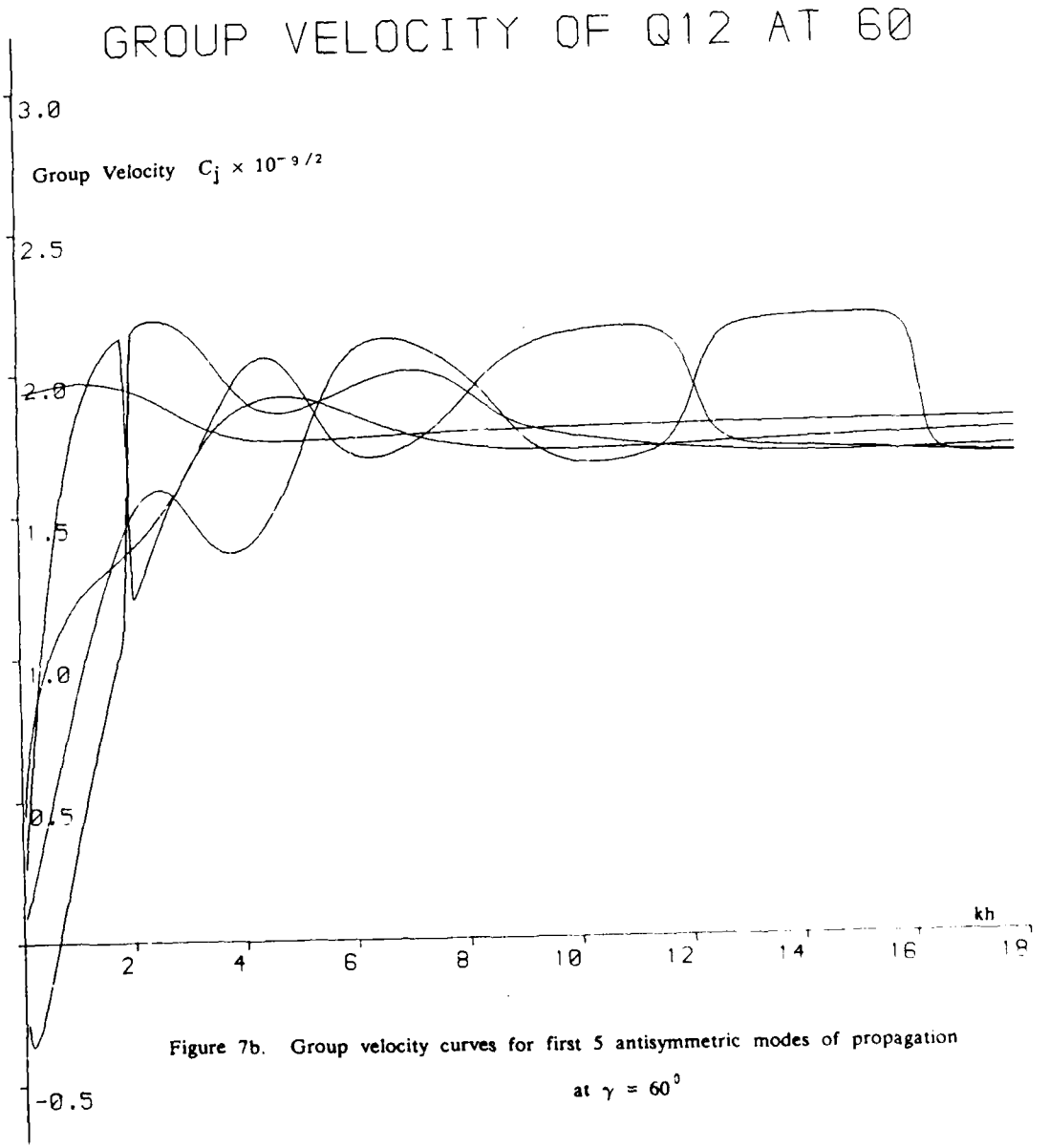

Figure 7b. Group velocity curves for first 5 antisymmetric modes of propagation at $\gamma = 60^0$

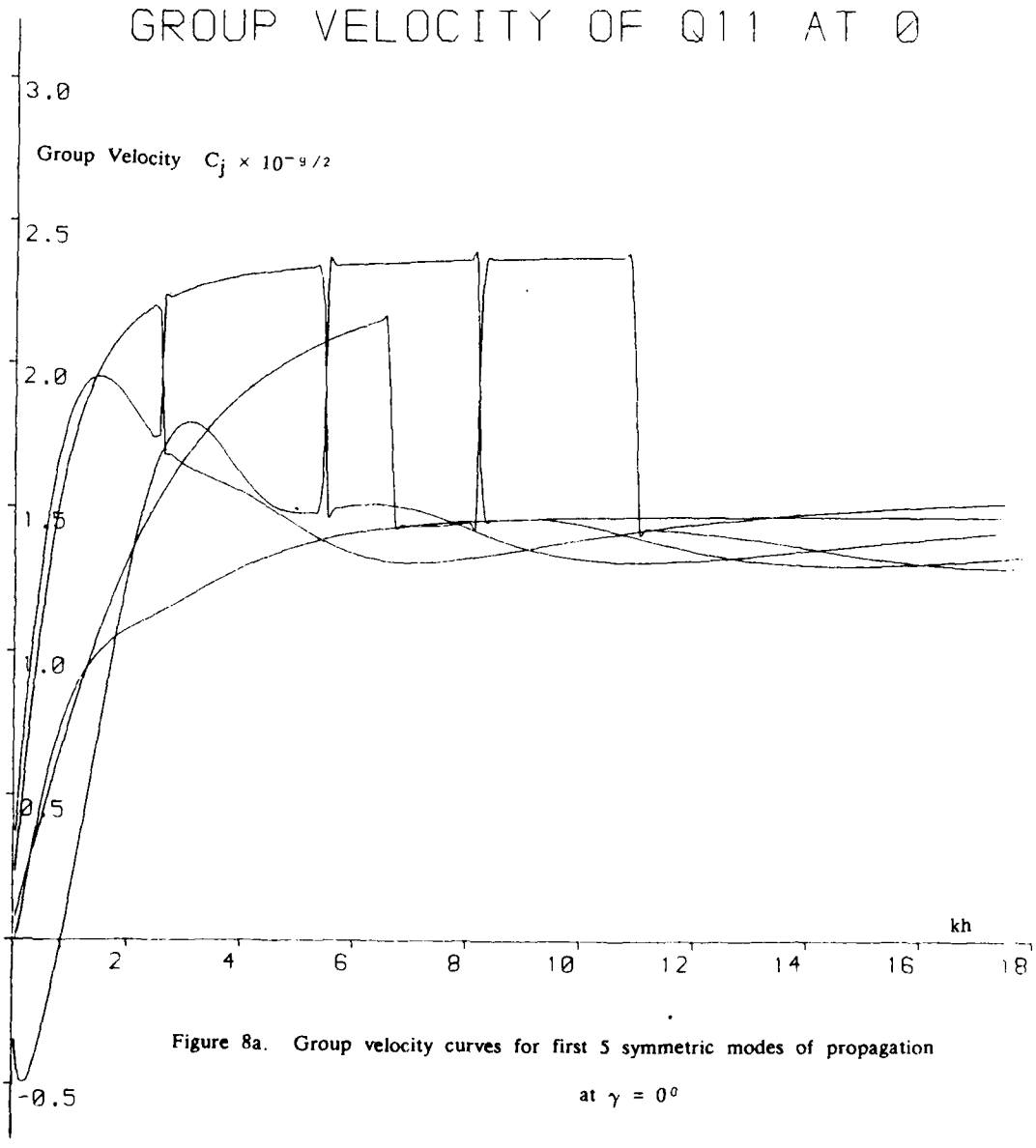

Figure 8a. Group velocity curves for first 5 symmetric modes of propagation at $\gamma = 0^0$

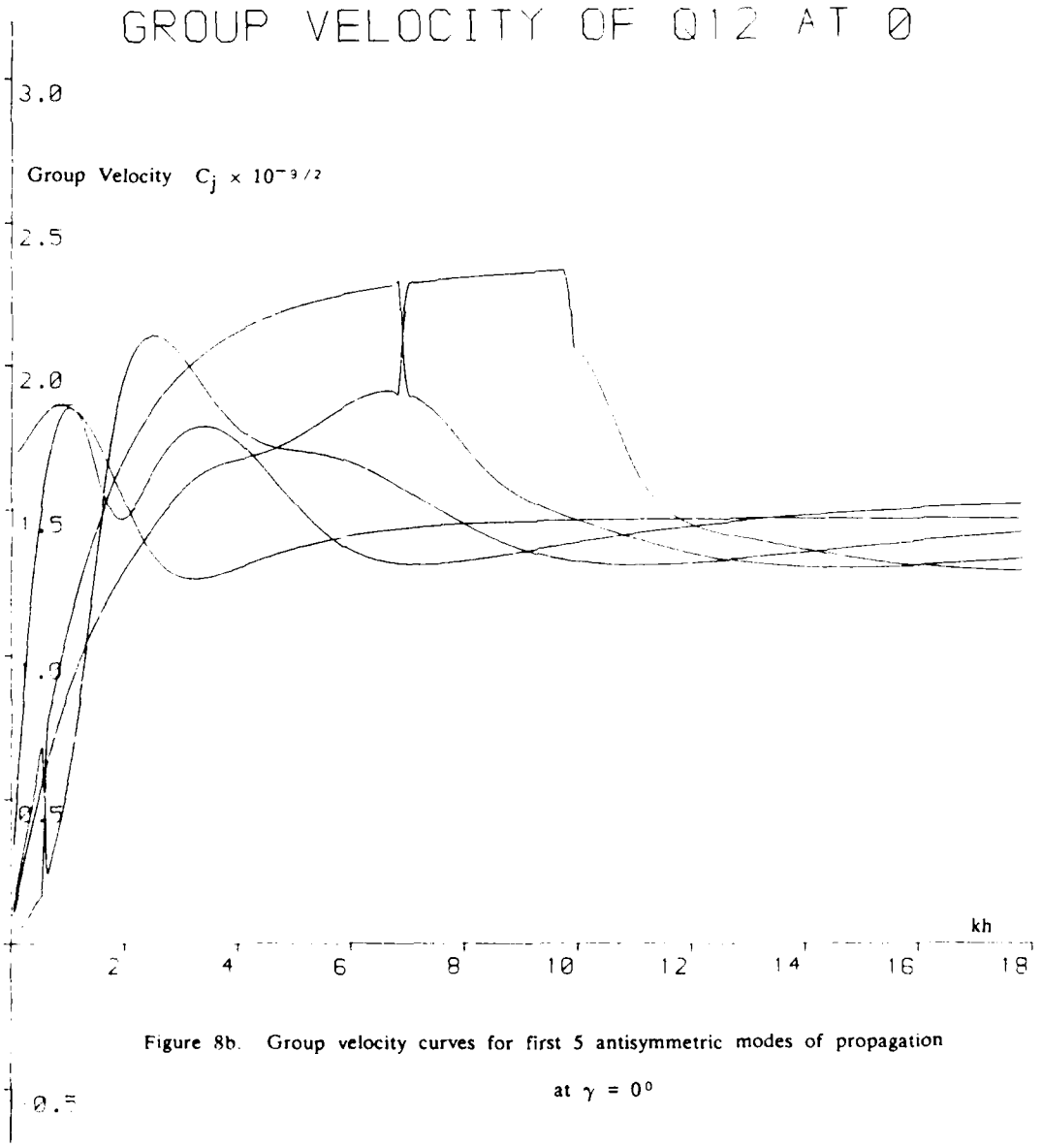

Figure 8b. Group velocity curves for first 5 antisymmetric modes of propagation at $\gamma = 0^0$

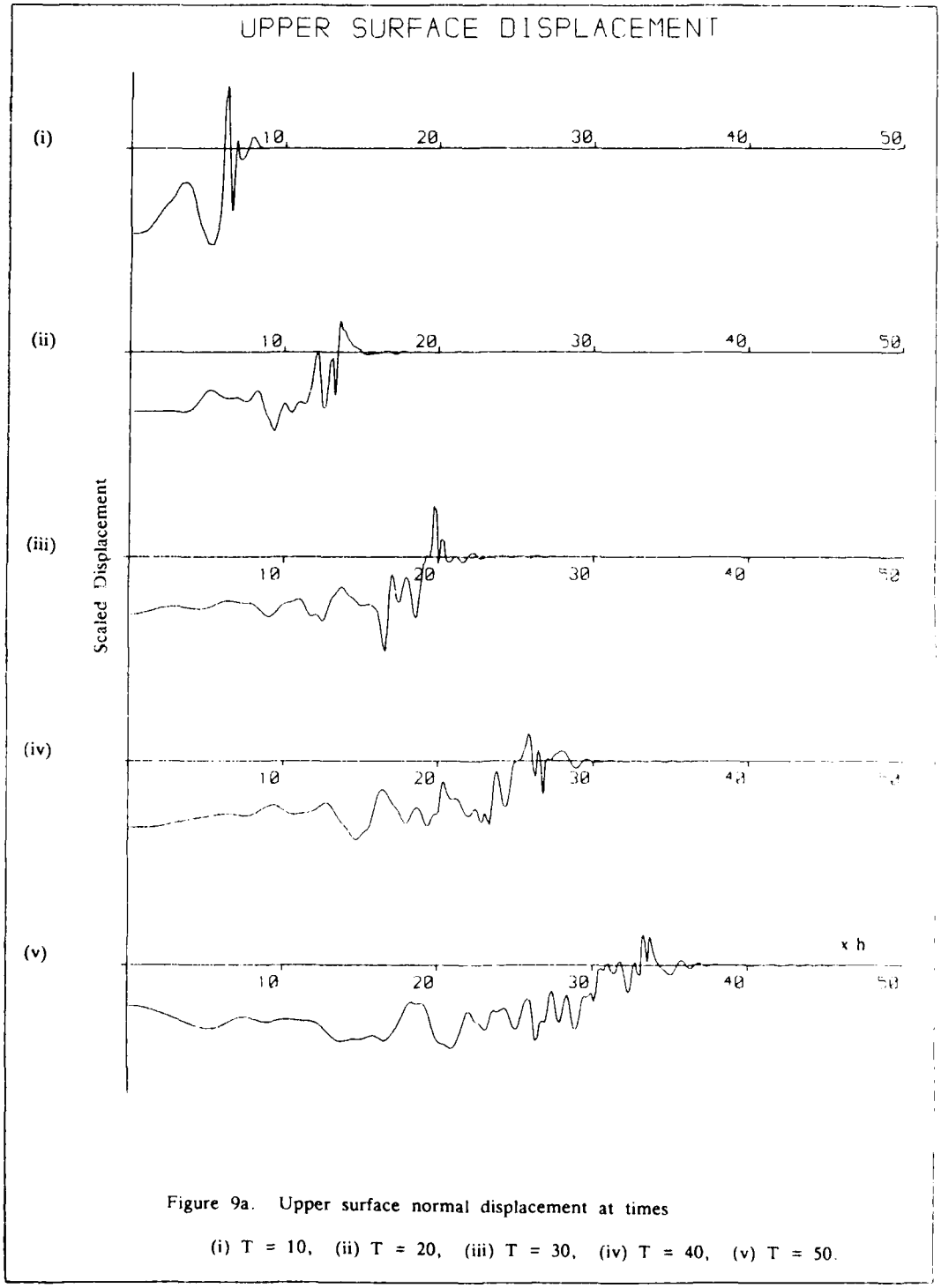

Figure 9a. Upper surface normal displacement at times

(i) T = 10, (ii) T = 20, (iii) T = 30, (iv) T = 40, (v) T = 50.

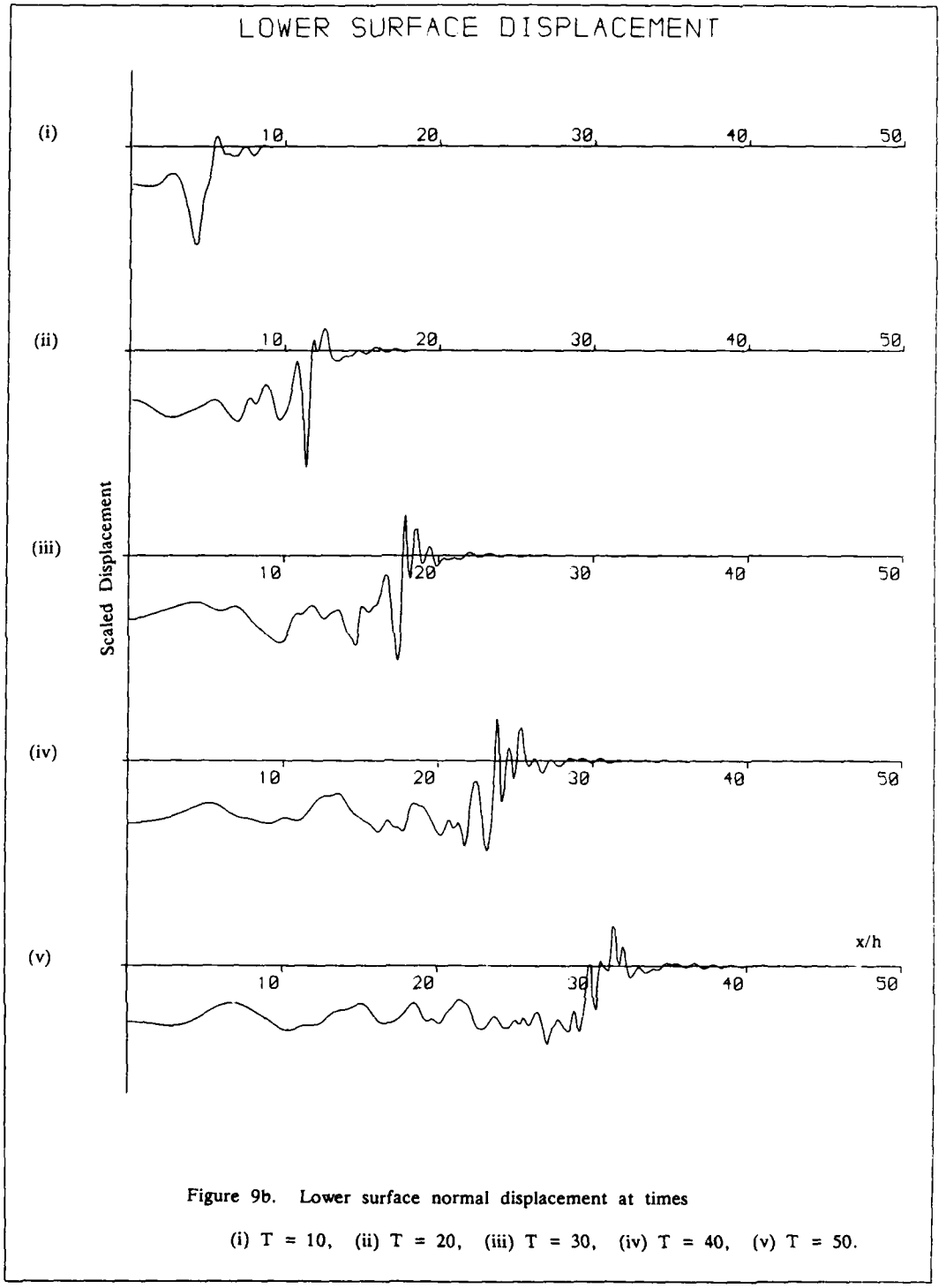

Figure 9b. Lower surface normal displacement at times

(i) T = 10, (ii) T = 20, (iii) T = 30, (iv) T = 40, (v) T = 50.

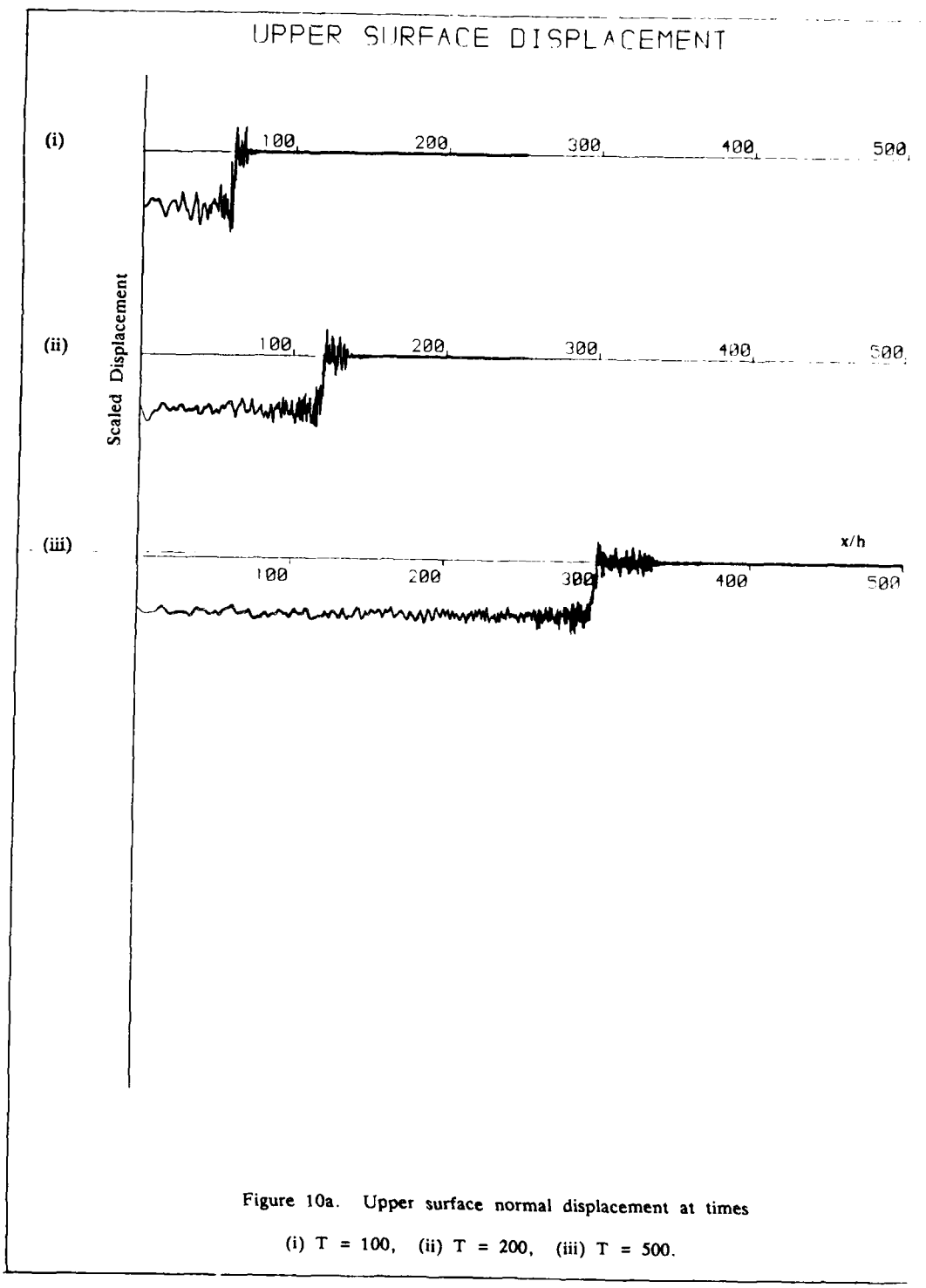

Figure 10a. Upper surface normal displacement at times

(i) T = 100, (ii) T = 200, (iii) T = 500.

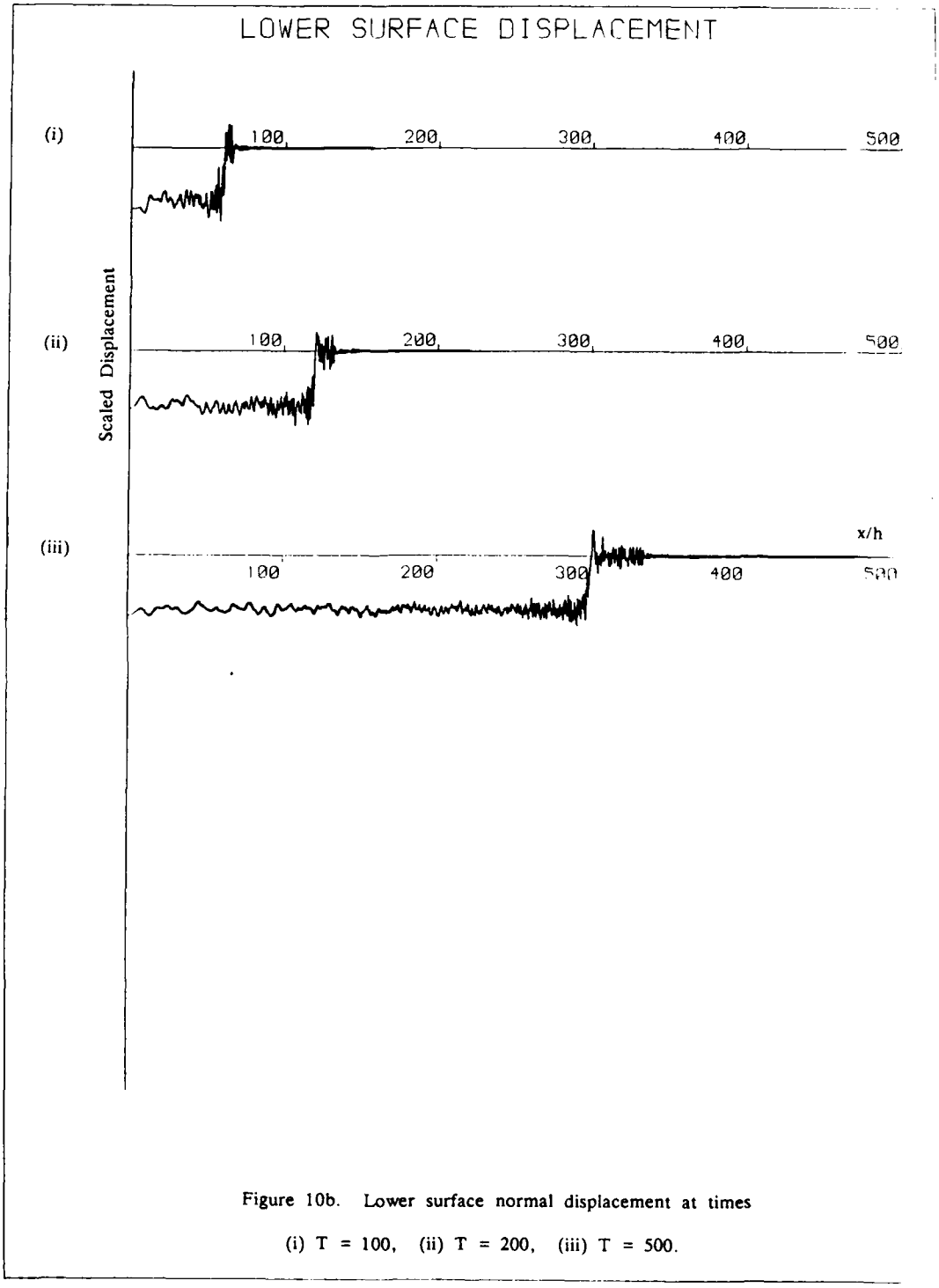

Figure 10b. Lower surface normal displacement at times

(i) T = 100, (ii) T = 200, (iii) T = 500.

(a)

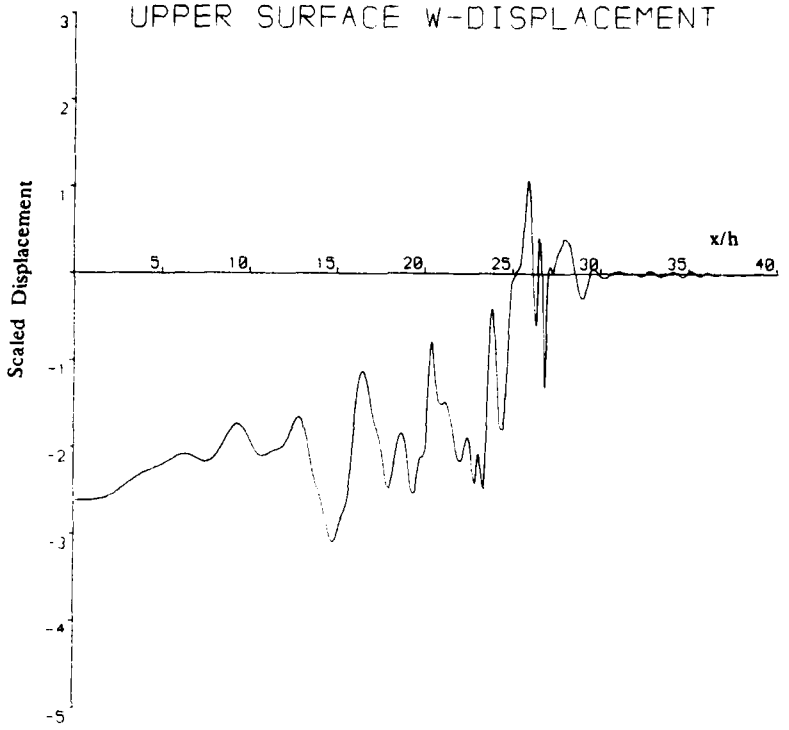

(b)

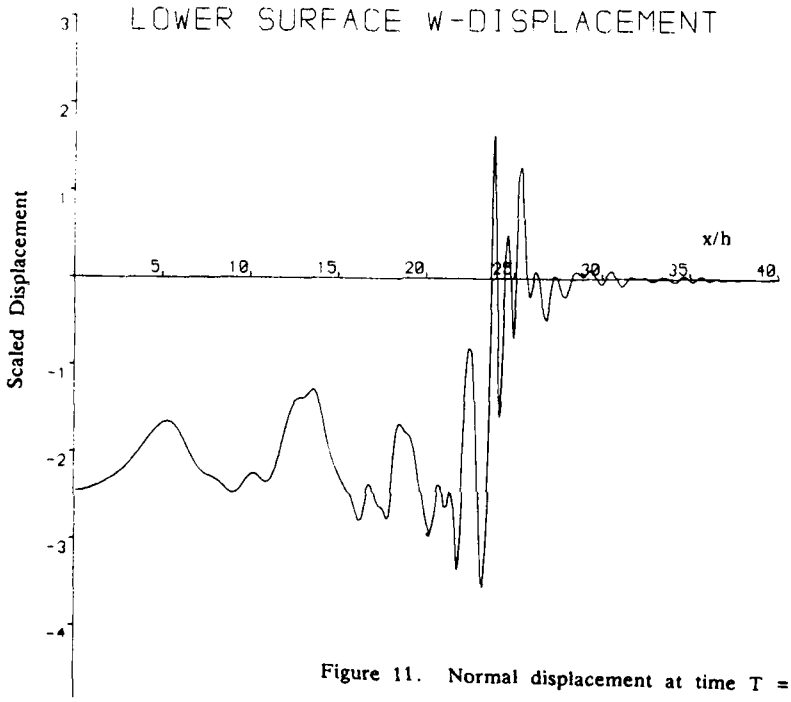

Figure 11. Normal displacement at time T = 40

(a)

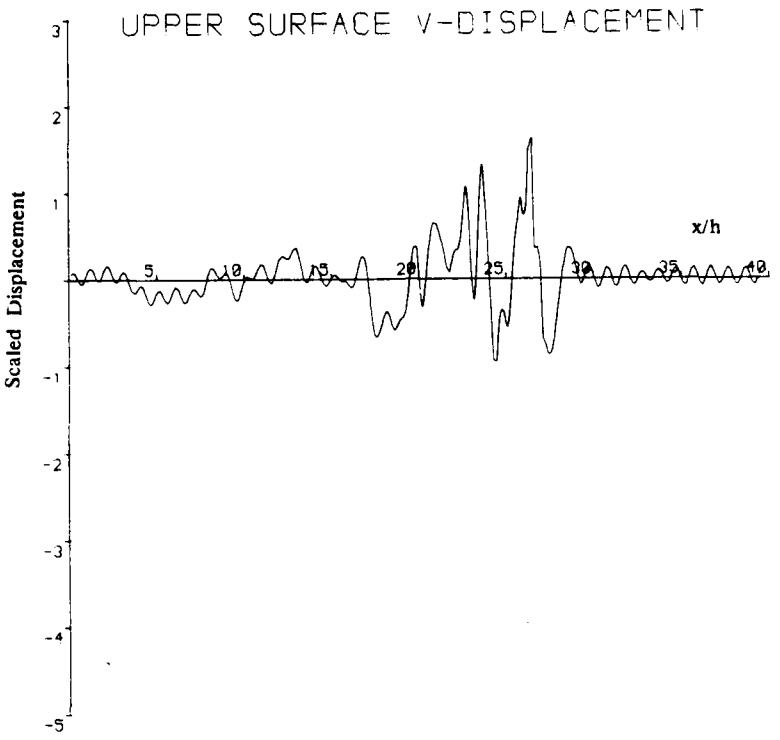

(b)

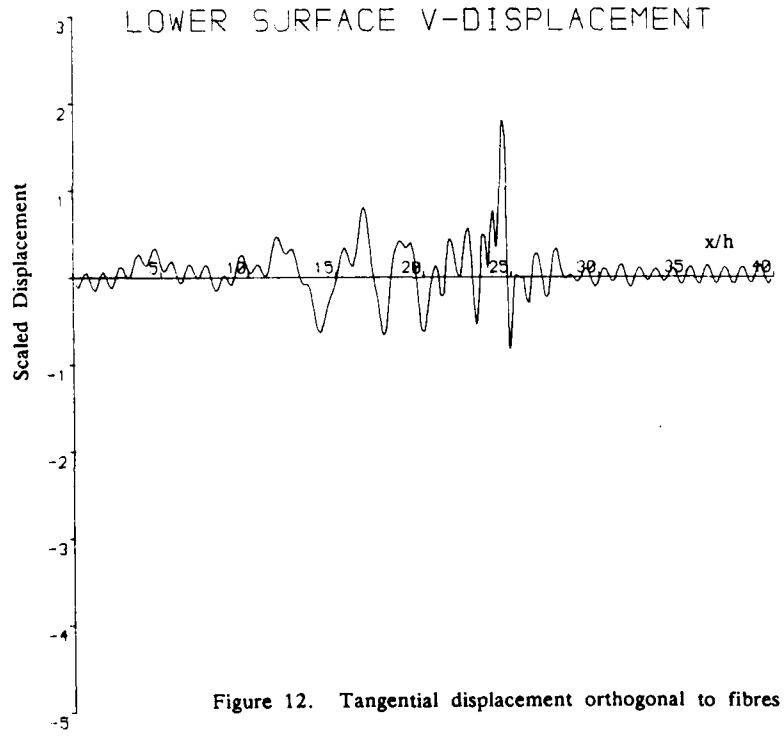

Figure 12. Tangential displacement orthogonal to fibres at time T = 40

(a) Upper surface (b) Lower surface

(a)

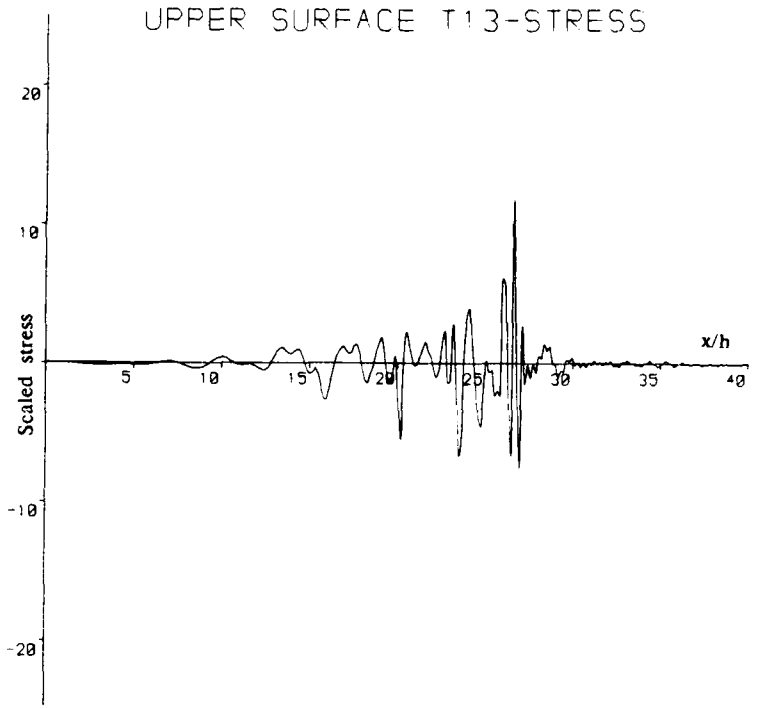

(b)

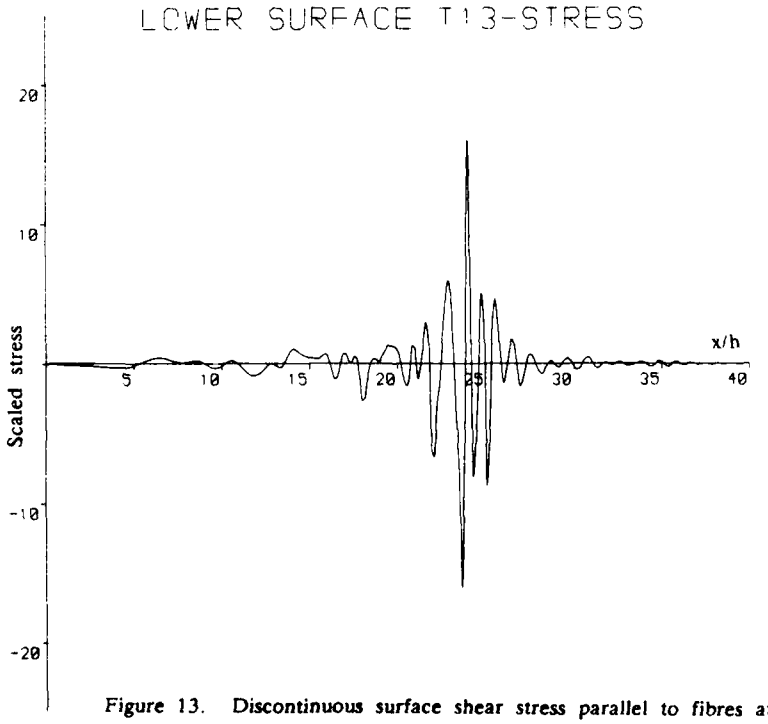

Figure 13. **Discontinuous surface shear stress parallel to fibres at T = 40**

(a) Upper surface **(b) Lower surface**

(a)

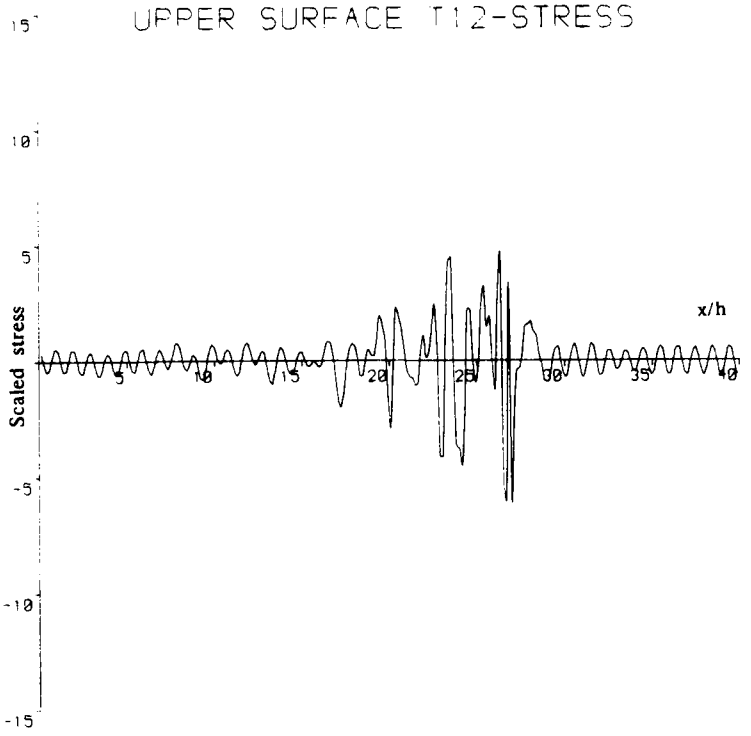

(b)

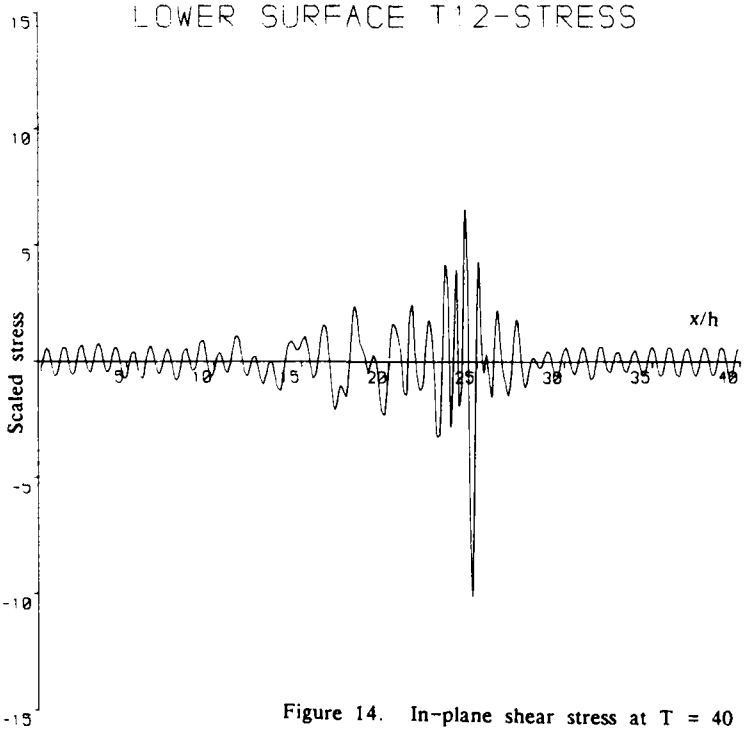

Figure 14. In-plane shear stress at T = 40

(a) Upper surface (b) Lower surface

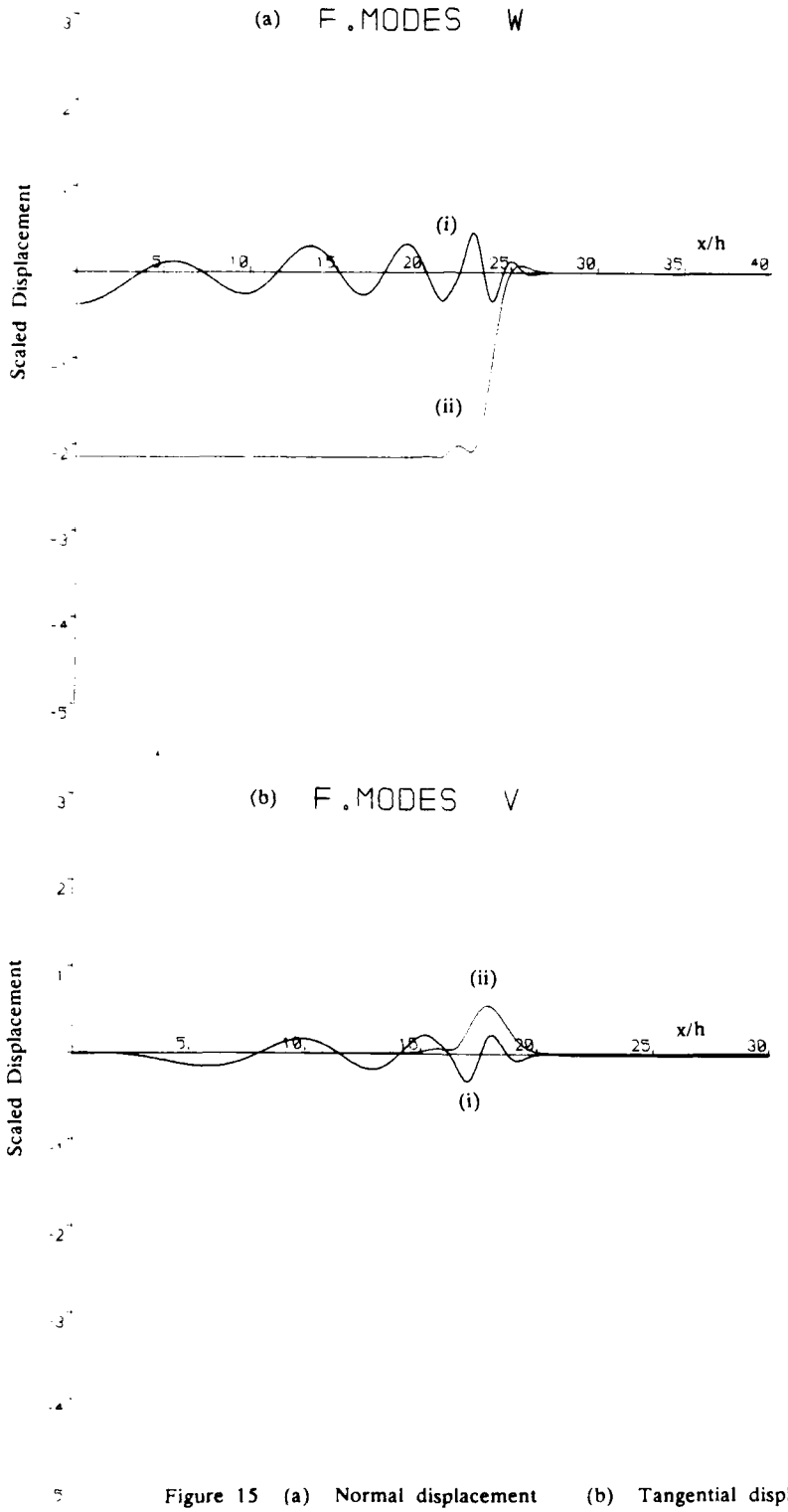

Figure 15 (a) Normal displacement (b) Tangential displacement at the upper surface arising from fundamental modes of (i) symmetric and (ii) antisymmetric motion at T = 40.

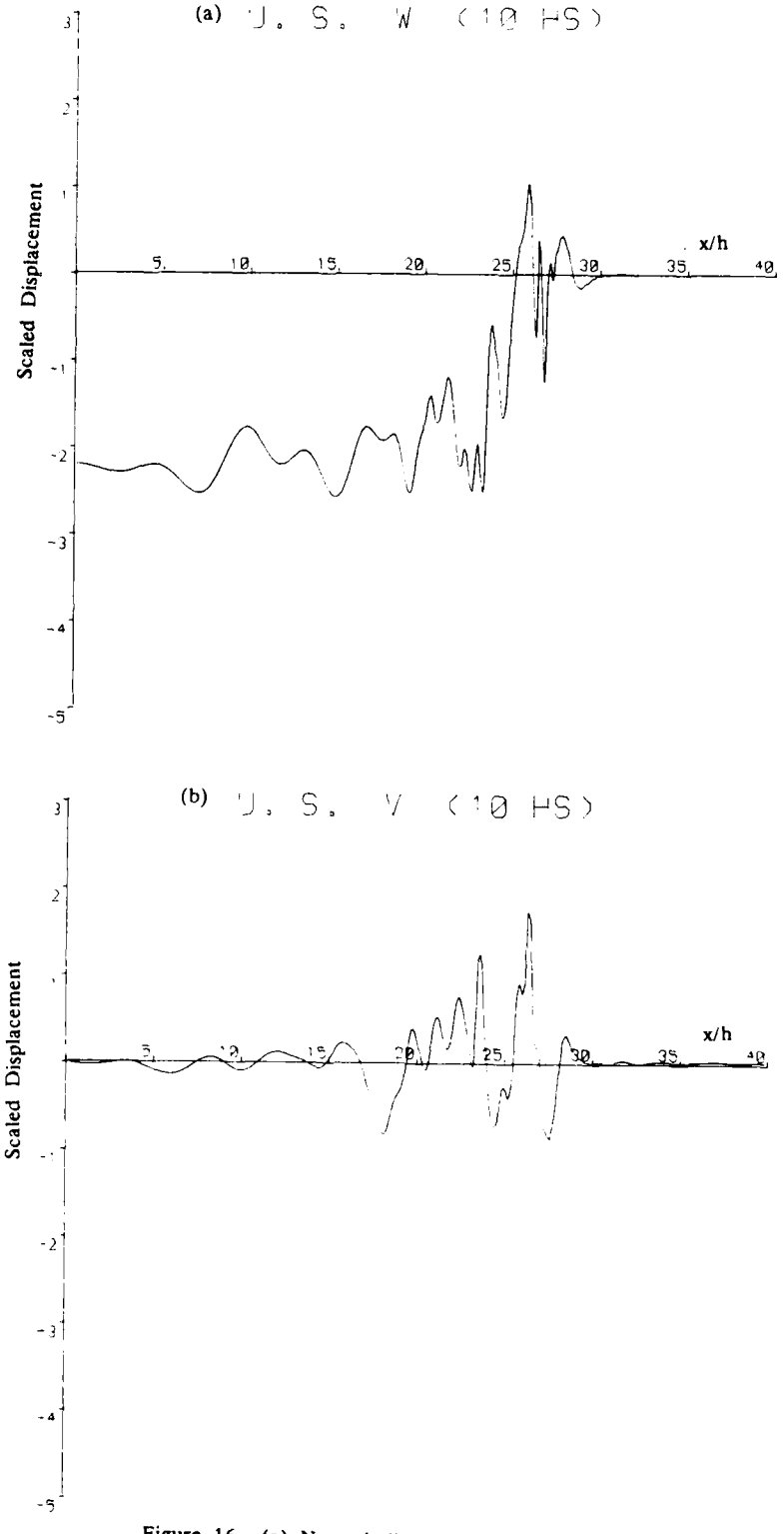

Figure 16 (a) Normal displacement (b) Tangential displacement at upper surface arising from first ten harmonics of dispersion equation at T = 40.

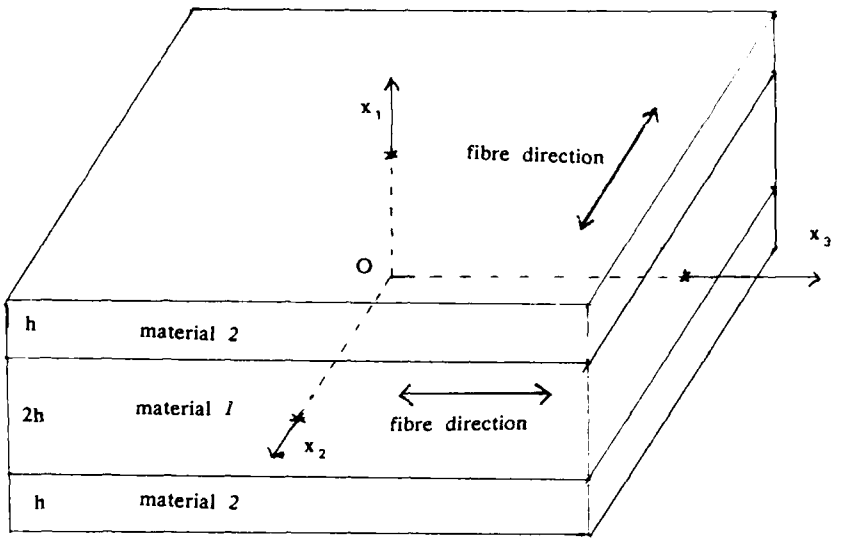

Figure 17 Section of unit cell.

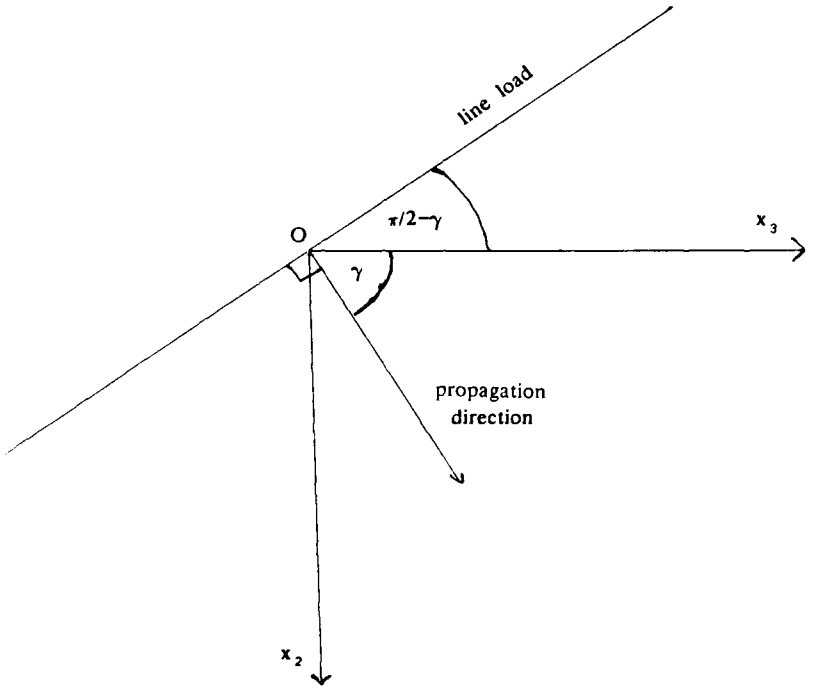

Figure 18 Geometry of impact problem.

END

DATE
FILMED

8 88